Accepted Manuscript

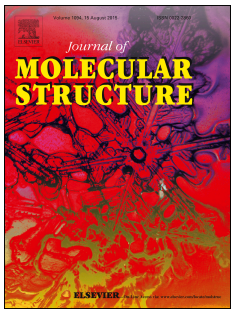

Synthesis, molecular structure, quantum chemical analysis, spectroscopic and molecular docking studies of *N*-(Morpholinomethyl) succinimide using DFT method

K. Sarojinidevi, P. Subramani, Mani Jeeva, N. Sundaraganesan, Maria SusaiBoobalan, G. VenkatesaPrabhu

PII: S0022-2860(18)30926-8

DOI: 10.1016/j.molstruc.2018.07.101

Reference: MOLSTR 25506

To appear in: *Journal of Molecular Structure*

Received Date: 5 May 2018

Revised Date: 18 July 2018

Accepted Date: 28 July 2018

Please cite this article as: K. Sarojinidevi, P. Subramani, M. Jeeva, N. Sundaraganesan, M. SusaiBoobalan, G. VenkatesaPrabhu, Synthesis, molecular structure, quantum chemical analysis, spectroscopic and molecular docking studies of *N*-(Morpholinomethyl) succinimide using DFT method, *Journal of Molecular Structure* (2018), doi: 10.1016/j.molstruc.2018.07.101.

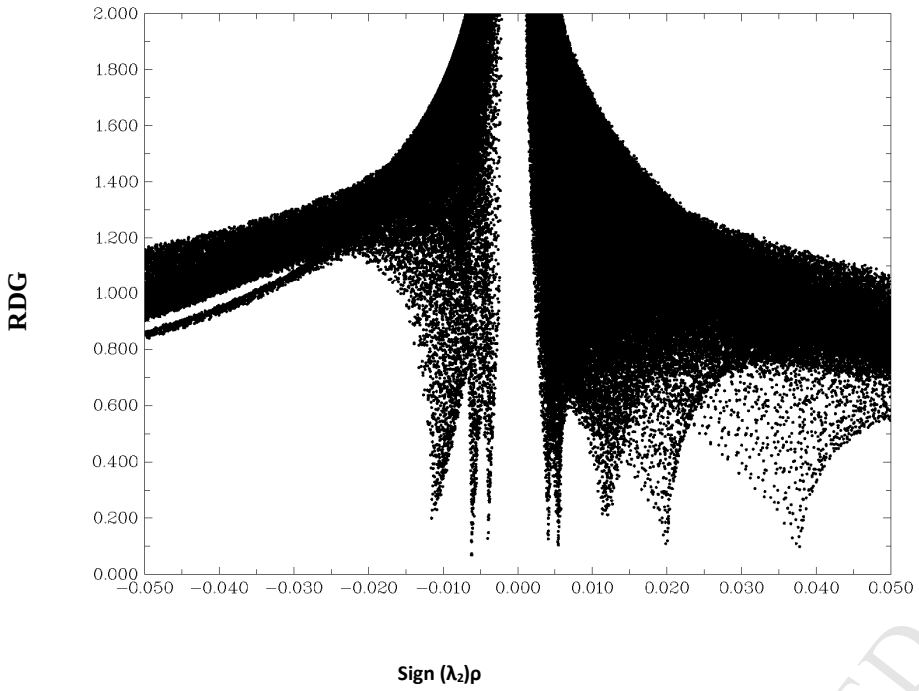

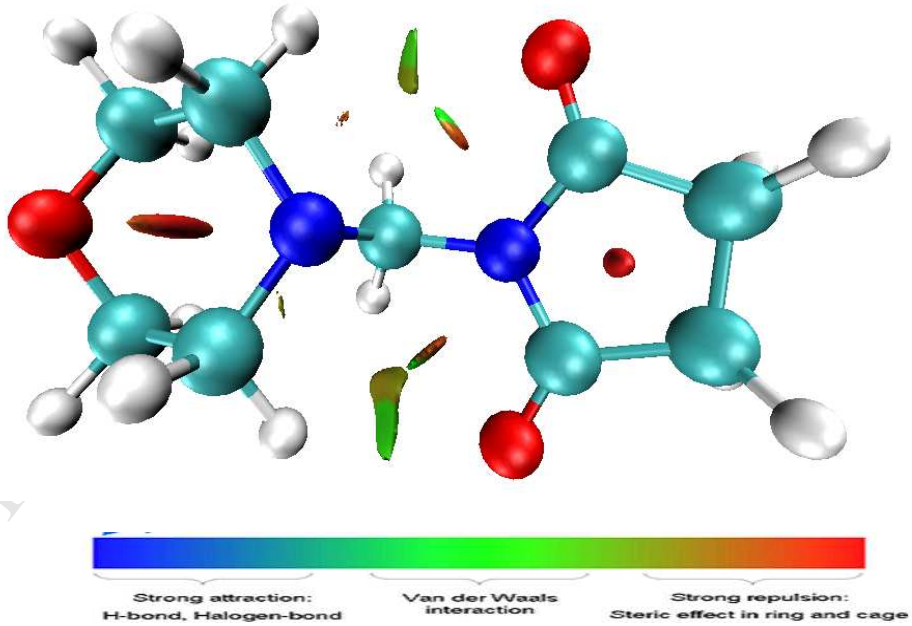

Synthesis, Molecular structure, Quantum chemical analysis, Spectroscopic and Molecular docking studies of N-(Morpholinomethyl) succinimide using DFT method

K.Sarojinidevi[a], *P. Subramani*[a]*, *Mani Jeeva*[b], *N. Sundaraganesan*[c], *Maria SusaiBoobalan*[d]

G. VenkatesaPrabhu[e]

[a]Department of Chemistry (Engg.), Annamalai University, Annamalai Nagar, 608 002 Chidambaram, Tamil Nadu, India.

[b]Department of Chemistry, National Institute of Technology, Tiruchirappalli-620015, Tamilnadu, India.

[c]Department of Physics (Engg.), Annamalai University, Annamalai Nagar, 608 002 Chidambaram, Tamil Nadu, India.

[d]Department of Chemistry College of Natural and Computational Sciences (CNCS),Haramaya University, Harar, Dire Dawa, Ethiopia.

[e]Department of Chemistry, National Institute of Technology, Tiruchirappalli - 620015, Tamilnadu, India.

ABSTRACT

N-(Morpholinomethyl) succinimide (SMF) bearing the empirical formula $C_9H_{14}N_2O_3$, has been synthesized by using the mannich condensation reaction. On considering its extensive pharmaceutical usage and medicinal value, we investigated its chemical structure and composition by employing various spectral techniques like ^1H, ^{13}C NMR, UV-Visible spectroscopy, FT-IR, FT-Raman and TG/DSC techniques. Density Functional Theory (DFT) computation was adopted to study the electronic structure of the SMF molecule. Incorporating the VEDA 4 package, Total Energy Distribution (TED) was computed for vibrational assignment. In order to find out the strength and stability of the molecules an analysis based on the Natural Bond Orbital (NBO) was carried out. Gauge-Independent Atomic orbital (GIAO) was employed to confirm whether the ^1H and ^{13}C NMR spectrum could show the chemical shift values. Frontier molecular orbitals in order to investigate the forbidden energy gap, viz., HOMO-LUMO were calculated and the λ_{max} values were observed. Frontier molecular orbitals were mainly identified which contributed the atomic orbitals. Based on the chemical activity, mapping of the figure was carried out on molecular electrostatic potential. The nature of molecular interaction was ascertained for

molecular docking studies in which the biological protein system was reported. Based on the results, a suitable mechanism, its protein binding mode and drug action were presented. Molecular docking results suggested that the SMF molecule might exhibit inhibitory activity against the lung cancer protein.

Keywords; Charge analysis; DFT; Moleculardocking; N-(Morpholinomethyl) succinimide; Vibrational spectra; TED.

Corresponding author

1. Introduction

N-(Morpholinomethyl) succinimide(SMF), having the empirical formula $C_9H_{14}N_2O_3$, it has been synthesized by using the condensation of aldehyde, imide and secondary amine. The familiar morpholines molecules naturally or synthetically have a significant application of pharmacological and biological with a great range structure core of organic molecules [1]. It is reported that the morpholine is widely used as an important building block in the field of medicinal chemistry [2-4]. A new series of morpholine derivatives has been reported by Micheli et al. [5] as a selective DAD3 receptor antagonist along with the data related to *in-vitro* profile and pharmacokinetic. The presence of various nitrogen heterocyclic molecule in morpholine derivatives play an important role as they occur in nature and biologically active molecules, which carry the anti-inflammatory and antagonist properties and are used in some chemical transformations as chiral auxiliaries [6]. Apart from having pharmacological properties, the morpholines have their important application in a limited level as a simple bases catalyst such as N-alkylating agent, catalysts and chiral auxiliaries in many organic synthesized [7-13]. Pyrizinamide (morphozinamide), one of the derivatives of morpholinomethyl is found to have more potential treatment properties with cure of tuberculosis than the traditional pyrizinamide [14]. Several succinimide derivatives have significant biological activities such as antiepileptic and anticonvulsive, fungicidal and other pharmacological [15-19] activities. Nowadays, Mannich base compounds, in chemistry,

express many opportunities for resourceful molecular system of biologically active and it is dependent on the expectations and their needs. The Mannich base molecular structures provide interaction of transition metal ions, which is the most valuable region in the coordination chemistry. Varity of Mannich bases and their metal complex structures have their individual creativity of biological importance and they play an important role in various industrial applications. Bundgaard and co-workers have reported the application of N-Mannich bases structure containing amine for antibiotics prodrug forms [20]. For illustration, the salicylamide and aromatic amines with succinimide are presented in N-Mannich bases compounds, which are used to identify the prodrug of therapeutic significance. Many Mannich bases are offered with amazing biological activity. 1-[Anilino (phenyl) methyl] pyrrolidine-2,5-dione is a group of Mannich base and its transition metal complexes have a valuable microbial significance. The Mannich base molecular system of 1-[(pyridin-2-yl amino) methyl] pyrrolidine-2,5-dione have their own biological activity expressly performance on antioxidant property. The SMF is a white-crystalline powder which has a melting point in the range of 101 - 103℃. The compound SMF based on coarse aqueous suspension, has acidity level of PH 6.2- 6.5. The studies of the SMF, both experimental and biological have been conducted, but the vigorous literature survey reveals that there are no theoretical investigations made on SMF molecule mainly focusing on the part of molecular structure, spectral assignments, orbital, PDOS, electrostatic potential, thermodynamic properties and molecular docking. The current work is dedicated to get the theoretical and computational conclusion of the electronic structure, equilibrium molecular geometry, vibrational modes (IR and Raman), NMR chemical shifts, mass spectral analysis and TG/DSC techniques of the SMF molecule.

2.Experimental Details

2.1. Synthesis of 1-(morpholinomethyl)Succinimide (SMF)

N-(Morpholinomethyl)Succinimide (SMF) was synthesized by Mannich condensation reaction [21 - 23] among succinimide, morpholine and formaldehyde in 1:1:1 molar ratio. Succinimide (5.00g, 0.05M) and morpholine (4.5 ml, 0.05M) mixed with the less amount of ethanol was stirred until the content becomes homogenous. To this mixture 40 % formaldehyde solution (3.8ml, 0.05M) was poured slowly in drops, as the stirring action continued. Once the adding process was over, stirring continued for 2 h at 60°C and then it was made to cool in refrigerator. The solid mass obtained was rinsed using distilled water, desiccated and the final residue was recrystallized from acetonitrile to yield a colourless crystalline powder (Yield: 88 %).

Reaction Scheme: 1

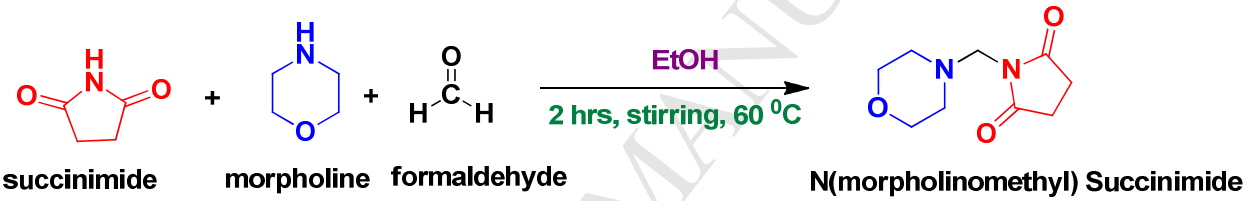

2.2. Experimental Method

The SMF molecule was synthesized and reported earlier [21- 23] and the Fourier Transform Infrared spectrum of SMF was recorded on a Perkin Elmer FT-IR spectrophotometer utilizing the KBr pellet (by mixing about 1–2 mg of the analyte with 300 - 400 mg of finely powdered KBr) strategy as a part of the range 4000 - 450 cm^{-1}as shown in Fig.1. Fourier Transform Raman spectrum was recorded on a BRUKER RFS 27 spectrometer utilizing 1064 nm excitation wavelength from a Nd:YAG Laser in the district 4000 -50 cm^{-1} as appeared in Fig.2. The laser yield for this solid specimen is about 100 mW. ^{1}H NMR spectra of SMF molecule were recorded on Bruker500 MHz Advance NMR spectrometer using TMS as an internal standard and its processing resonance frequency with the applied radio-wave frequency at 0 ppm in δ-scale (the chemical shift value) as presented in Fig.3(a). Furthermore, the sampling of the compound was done using highly polar protic solvent, dimethyl sulfoxide (DMSO). Proton decoupled ^{13}C NMR spectra were recorded on Advance NMR Bruker spectrometer 500 MHz, with an operating frequency of about 75 MHz, by using the deuterated dimethyl sulfoxide (DMSO) as a solvent as shown in Fig.3(b). TMS was used as an internal standard. The HRMS analysis was done using High Resolution Q-

TofMass, mass spectrometer as detector (Perkin Elmer), TurboMassver 5.4.2 software for data analysis. The GC parameters were found as split 10:1 injection; column: Elite-5MS (30m x 0.25 mm I.D, 250μm df); injection port temperature: 250 °C; carrier gas: helium; flow rate: 1 mL/min; oven temperature: initially 60 °C for 2 min, ramped to 300 °C at 10 °C/min, 300 °C for 6 min. The MS conditions found were as follows: transfer line heater: 240 °C; ion source temperature: 240 °C; electron impact ionization (EI) mode; ionization energy: 70 eV. Analysis was performed in scan mode, from 600 -10 amu at a speed of 1.5 scans/s. Solvent delay was set as 2.0 min as observed in Fig.4 (a). The obtained mass spectra were compared with commonly used EI-MS spectra libraries (NIST, Wiley 2008). TG/DSC study was engaged with the thermo gravimetric instrument TGA7 (Perkin Elmer) Q500 Hi-Res TGA from TA instruments), DSC7 (Perkin Elmer) Q200 Hi-Res TGA from TA instruments as shown in Fig.4 (b). UV-Vis spectrum was recorded in DMSO solvent by employing the Lambda-35 Perkin Elmer spectrophotometer as a part of the spectral locale of 1100-190 nm as shown in Fig.S1 (Supplementary information).The entire spectrum experiment was condensed at Indian Institute of Technology (IIT), Madras, India.

3. Computational Details

Density Functional Theory (DFT) calculations were employed in the Gaussian-09 program [24] package used in our study. The Becke three parameter hybrids functional method has been employed in the work. It consists of non-local exchange functional of Becke style three parameter sets and the non-local correlation functional of Lee, Yang and Parr [25, 26]. The triple-split valence Gaussian function usually along with polarization functional, for both bulky atoms and simple atom like hydrogen, 6-31G (d, p) basis sets have been involved in the calculations. The saddle- point or stationary points as the energy due to minima at the DFT level using harmonic vibrational analyses have been determined. The vibrational spectrum bands were performed on account of the corresponding total energy distribution (TED) calculated with the help of VEDA 4 program [27] while the GuassView program [28] was employed to give a visual presentation of the vibrational assignments. Natural Bond Orbital (NBO) analysis was adopted using NBO 3.1 program [29] incorporated in Gaussian09W at B3LYP/6-31G (d,p) level, to find the inter- molecular delocalization between the filled orbital and unfilled orbital and also to calculate the hyper conjugation. The gauge independent atomic orbitals (GIAO) method [30, 31] along with the B3LYP/6-31G (d,p) functional method was used to calculate the chemical shifts of the SMF molecule. ^{1}H and ^{13}C isotropic magnetic shielding (IMS) of every X atom (carbon or hydrogen) was

applied corresponding to the standard value of TMS, CSX = IMSTMS – IMSx. UV-Vis spectra and electronic properties of molecular orbital energies were simulated by Time-Dependent DFT (TD-DFT). The Density of states (DOS) was performed with the help of Gauss- sum 3.0 software program [32].

3.1. Prediction of Raman Intensities;

The theoretical Raman intensity (I_i^R) is simulated by calculating Raman spectrum which can be predicted using the formula [33] [34].

$$(I_i^R) = C(\nu_0 - \nu_i)^4 \nu_i^{-1} B_i^{-1} S_i \quad \text{----------} \quad (1)$$

Where the B_i is the temperature factor, which accounting for the intensity contribution of excited vibrational states and its denoted by the Boltzmann appropriation (B_i)

$$B_i = 1\text{-}\exp^{-(h\nu i / KT)} \quad \text{----------} \quad (2)$$

In this study, the I^R_i equation, ν_i is the frequency of laser excitation line and we have utilized the excitation frequency ν_0= 9398.5 cm^{-1}, which corresponds to the wavelength of 1064 nm of a Nd:YAG laser. The ν_i represents the frequency of normal mode (cm^{-1}), while the S_i is the Raman scattering activity of the normal mode Q_i. The I^R_i is assumed in arbitrary unit. In the above said equation, the h and k denote Planck and Boltzmann constants, C and T represent the speed of light and temperature in Kelvin, respectively.

4. Results and discussion

4.1. Molecular geometry

The complete geometrical optimization was accomplished by accepting the C1 point group symmetry. The optimized molecular constitution of the most stable structure of SMF molecule as B3LYP/6-31G (d, p) basic set is shown in Fig.5. By using B3LYP/6-31G (d, p) method the structural parameters like bond lengths, bond angles and dihedral angles of the titled molecule have been computed and optimized. The X-ray crystal data of the titled molecule [21] are compared with the results obtained and presented in Table1. All the bond lengths and bond angle values show small deviation when compared to the calculated XRD values obtained by using the B3LYP/6-31G (d, p) basis set. The experimental values show the molecule as solid state, whereas the theoretical calculation has predicted an isolated molecule in gaseous state. The SMF molecule consists of electronegativity nitrogen atoms bonded with the carbon (C8) atom of morpholine moiety. The carbonyl group (C═O) along with the succinimide moiety by other termination acts as an electron acceptor. The charge transfer involves over the π-conjugation among the electron contributor and acceptor groups.

This SMF molecule contains fourteen C-H bonds, five C-C bonds, two C═O bonds, six C-N bonds and two C-O bonds. The five membered rings consist of two dione at C1=O2, C5=O6 and lie in the range, obtained for DFT calculation 1.215 Å, 1.214 Å which are associated with experimental data 1.201 Å and1.211 Å available from the literature [22]. The C10-O9 and C14-O9 bond length calculated by B3LYP/6-31G (d, p) method are of the same value of 1.425 Å which is slightly deviated from the experimental data of a related molecule by 1.423Å and 1.409Å [21] respectively. The calculated C-N bond length in the morpholine ring are C8-N12=1.444 Å, C11-N12 = 1.467 Å, C13-N12= 1.468 Å and in the succinimide ring are C1-N7 = 1.392 Å, C5-N7 =1.393 Å, C8-N7 = 1.473 Å by B3LYP/6-31G (d, p). These values are similar to the related experimental values such as 1.430, 1.449, 1.4535, 1.387, 1.375 and1.482 Å. The C-N bonds reveal impartial double bond properties in this fragment which are compared to the normal value of the single C-N bond (1.47 Å) and C=N bond 1.22 Å assemble given in the literature [23]. The morpholine is elongated due to the presence of C-C bond length exactly at the location of nitrogen and oxygen substitutions, which gives bond lengths C10-C11 and C13-C14 leading to 1.531 Å and similarly in the succinimide C1-C3and C4-C5 lead to 1.527Å and C3-C4 lead to 1.537 Å while the observed values are 1.497, 1.495, 1.498 and 1.494, 1.510 Å. The calculated C–C bond length in succinimide ring varies from 1.527-1.537Å by the B3LYP/ 6-31G (d, p) which synchronize with recorded data (1.494-1.510Å). The C- C bond lengths of the morpholine ring record the value as 1.531 Å. The corresponding values are very near to experimental XRD values (1.495-1.497 Å). The bond length C3-C4 has the maximum value (C3-C4=1.537 Å by B3LYP/ 6-31G (d, p), 1.510 Å by XRD) compared to the other C-C bond lengths. The electron deficient (carbonyl) group present in the succinimide ring, due to the symmetry of the cyclic system is not disturbed. The bond length C1-C3 =1.527 Å and C4-C5 =1.527Å is shorter than the C3- C4 =1.537Å which is measured using DFT method at the other substitution. The maximum contraction in the succinimide ring angle C3-C4-C5 is computed at 105.1° and the experimental result shows good correlation with this value at 105.2°. The C-H bond length of the succinimide and morpholine ring varies from 1.092 Å -1.105 Å which is found slightly greater than the experimental value 0.970 Å. Whereas, small increment occurs in morpholine ring, the C-H bond lengths C10-H21=1.095Å, C10-H22=1.105Å, C11-H23=1.098Å, C11- H24=1.094Å, C13-H25 =1.098 Å, C13-H26 =1.094 Å, C14-H27 = 1.105 Å, C14-H28=1.095 Å have equal values for C10-H22 and C10-H21of B3LYP/ 6-31G (d, p).

4.2. Mulliken population analysis

Mulliken charge distribution of the SMF molecule was analyzed using the B3LYP/6-31G (d, p) method. In order to assigned its compositional molecules such as N-methyl morpholine and N-methyl succinimide. The results are summarized in Table S1 (Supplementary information). The horizontal bar diagram of comparative Mulliken charge distributions is displayed in Fig.S2 (Supplementary information). The comparison of Mulliken charge distribution with the intact SMF molecule and its separated N-methyl morpholine indicate the Mulliken population analysis as almost similar in the cyclic system and all the carbon atoms and oxygen atoms show negative charge in both the SMF molecule and the N-methyl morpholine moiety; whereas the atoms C8 exhibit some deviation between the SMF molecule and the N-methyl morpholine. This confirms the impact of the attachment of the N-methyl succinimide ring in the SMF molecule. Similarly, the N-methyl succinimide ring in the SMF molecule displayed deviation of Mulliken charges from that of the separated N-methyl succinimide moiety in the atom C8 space only. The atomic charge of C8 in the SMF molecule shows positive compared with that of the separated N-methyl succinimide moiety. Carbon atoms C1, C2 (having carbonyl group), C8 (attached with nitrogen atoms) C10, C14 (attached with oxygen atoms) are positive while other carbon atoms are negative and among these, C1 and C5 are most positive which occurs due to the presence of a carbonyl group. From the SMF molecule, the carbon atoms are nearly equally negative, but C11 and C13 found to be highly negative charged which naturally occur with specific movement of electrons from N12 to carbon (morpholine ring). Atoms C10 and C14 in the SMF molecule were computed with the less positive charge due to the presence of the oxygen atom. By sharing the electron with neighbouring carbon atoms the hydrogen atoms found in SMF molecule show positive results. The Mulliken atomic charges of the succinimide group hydrogen atom H16 and H18 are higher than the morpholine group and the methylene group hydrogen. It denotes the succinimide group hydrogen atoms as found more acidic than the morpholine group and methylene group hydrogen atoms. However, the high value of 0.15038 and 0.15039 for H16 and H18 respectively with the B3LYP/6-31G (d, p) basis set. Mulliken charge distribution analysis found the carbonyl, oxygen and nitrogen groups in the SMF molecule as contributing factors positively to its biological activity.

4.3. Dipole moment of SMF

The dipole moment of SMF molecule has the value of 2.0423 D representing the vector components of the dipole moment along with Cartesian coordinates are summarized in Table S2 (Supplementary information). The dipole moment value, on the whole is found far greater when compared to water, [(H_2O) μ =1.85 D]. The dipole moment of morpholine [μ =1.71 D] is found lesser than that of title molecule while succinimide [μ =2.22 D] which is greater than that of title molecule [35, 36]. Being a highly polar in nature, the SMF molecule is found to be soluble, easily in polar solvents (methanol, ethanol, n-propanol, isopropanol, n-butanol, acetone, DMSO, DMF and $CHCl_3$) and this activity is found absent in the case of certain polar organic compounds such as water, ether and partially soluble in CCl4, benzene and acetonitrile [22]. The direction of dipole moment vector co-ordinates of SMF is shown in Fig.S3 (Supplementary information). The electric dipole moment components data along with cartesian coordinates, are considered as the magnitude of the total dipole moment is preferably pointed towards the negative Z-direction, mainly consider as the electron withdrawing group such as oxygen atoms placed at morpholine ring, carbonyl group at C1 and C5 and the Nitrogen atom found in N-CH_2-N are all present in the positive X and Z-direction. The remaining atoms are slightly often circulated among the additional two Cartesian axes. The above inferences indicate an unsymmetrical charge separately distributed within the molecule, but only partially extent around the molecule.

4.4. Vibrational analysis

The title SMF molecule has C1 symmetry and consisting of 28 atoms with 78 normal modes of vibration, which may be distributed as 53 in-plane and 25 out-of-plane bending vibrations. It is concluded that the FT-IR and FT-Raman are active on the vibrational modes. The comparison of computed FT-Raman and FT-IR bands with experimental wavenumbers and vibrational assignments are summarized in Table 2 and the theoretically constructed FT-IR and Raman spectrum are shown in Fig.S4 (Supplementary information). The computed wavenumber are scaled by 0.967 which was recommended by A.P.Scott [37].

4.4.1. C=O vibrations

In the case of five membered cyclic systems [38], the carbonyl group frequencies are shown in the assortment 1830-1800 cm^{-1} and 1790-1740 cm^{-1}. The experimentally reported values of our studied molecule reflect strong and very strong band at 1765$cm^{-1}$and 1737 cm^{-1} respectively in the FT-IR spectrum and very strong peak at 1769 cm^{-1} in the FT-Raman spectrum, which are assigned as C=O stretching vibration. In the current studies, we have noticed theoretically predicted strong, intense C=O stretching vibration corresponding to a

wavenumber of 1800, 1740 cm^{-1}. The TED for these vibrations, show 86 and 87% contribution suggests that the above values are pure stretching vibrations. The observed value of C=O group vibration is slightly lower than the theoretically calculated frequency and it is indicated that the conjugation of the carbonyl(C=O) bond in the succinimide ring, increase the single bond character, which gives a minimum value for carbonyl group stretching wavenumbers [39]. In the FT-IR spectrum, the weakest band was observed at 934 cm^{-1} which synchronizes to the theoretical wavenumber at 961 cm^{-1} and is related to the C= O stretching vibration mode which is mixed with C-N and C-C stretching mode. In the SMF system, the C=O in-plane and out-of plane bending vibrations are observed at 536 and 557 cm^{-1} in FT-IR as the weak and very weak bands respectively. Similarly, the vibrations at 532 and 561cm^{-1} in FT-Raman as the weak and strong band respectively correlate well with the calculated counterpart at 540 and 557 cm^{-1} with a TED contribution of 64 and 42% respectively. It is coupled with C-C stretching and bending of CNC, in- plane of CCCH vibration mode. The main attribute vibration of cyclic ether in the sequence from 1150–1085 cm^{-1} corresponds to the C-O-C asymmetric stretching [40, 41]. The computed C-O-C asymmetric stretching vibrations are observed at 1103 cm^{-1} and found to have perfect concurrence with the experimental FT-IR value of 1110 cm^{-1}.

4.4.2.C-N vibration

The identity of the C-N vibrations occurring in molecules, are generated to be complex and allows several bands to get mixed in the following region. The C-N stretching vibration is found 783 cm^{-1} in FT-Raman spectrum and in FT-IR the peak shows at 781 cm^{-1} which are correlated well with the computed value at 780 cm^{-1} by B3LYP/6-31G (d, p) method with 58 % of TED impact. In addition to these vibrations, the C–N–C, N–C–N and C–C–N bending vibrations (i.e. in plane and out-of-plane) have been designed by TED, showing good concurrence with recorded observed data. The C-N in-plane bending harmonic vibrations computed at 1359, 1338, 1194, 620, 470, 468, 254 cm^{-1} by B3LYP/6-31G (d, p) method show excellent agreement with the FT-IR band at 621 cm^{-1} and FT-Raman bands at 608, 216 cm^{-1} are assigned to C-N in-plane bending vibrations. In the SMF molecule, the C-N torsion and out-of plane bending vibrations are observed at 1245, 883, 557 and 428 cm^{-1} in FT-IR and at 1308, 884, 561 and 413 cm^{-1} in FT-Raman which correlate well with the theoretical counterpart at 1319, 1235, 893, 557 and 430 cm^{-1} with a TED contribution of ~ 40%.

4.4.3. CH_2 vibration

The CH_2-stretching region of morpholine is remarkably similar to that of piperazine, except the changes in comparative intensities. The oxygen atom having a lone pair plays an analogous role as that of nitrogen in changing the confident CH_2 bands [42]. The intense observed peak presented in the range such as 2800 -3000 cm^{-1} are considered with overlapping due to the absorption peaks of stretching vibration of the CH_2 group [43]. The asymmetric CH_2 stretching vibration usually observed in the range 3000 -2900 cm^{-1} while the CH_2 symmetric stretch appears to be 2900 and 2800 cm^{-1} [44, 45]. The bands at 2861 in FT-Raman and 2880, 2867 cm^{-1} in the FT-IR is assigned to CH_2 symmetric stretching vibrations. The medium and strong intensity band at 3014, 2986, 2958 and 2944 cm^{-1} in FT-Raman and a strong to very weak bands at 2986, 2961, 2938 and 2939 cm^{-1} in FT-IR are assigned to CH_2 asymmetric vibrations of SMF molecule. The CH_2 symmetric and asymmetric stretching wavenumber of theoretical anharmonic frequencies by B3LYP method show best affiliation with the recorded spectral data. The further related bands of CH_2 group are tabulated in Table 2. The computed frequency of twisting and rocking of the CH_2 vibrations, show a perfect concurrence with the experimental observation values by B3LYP/ 6-31G (d, p).

4.4.4. C-C vibrations

For our SMF molecule, the C-C stretching vibration was predicted theoretically to appear in the lower frequency range such as 1012 and 853 cm^{-1}. The C-C stretching was observed at 985and 858 cm^{-1} as a strong band in FT-IR and in FT-Raman observed at 984 and 854 cm^{-1} which coincides with the theoretical counterpart value at 856 cm^{-1}. The very strong peak was obtained at 632 cm^{-1} in the FT- IR and observed at 661 cm^{-1} as a very strong, intense band in FT-Raman correlate well with the theoretical wavenumber at 651cm^{-1} which occur due to the presence of CCC in-plane bending vibration. The CCCC out of plane bending vibration is computed at 84cm^{-1} theoretically which correlates well with FT-Raman at 76 cm^{-1} as a very strong band with a TED vibration mode of 86 %.

4.5. NBO analysis

The Natural Bond Orbitals (NBO) calculations were predicted with NBO 3.1 program [29] as appliance in the Gaussian 09 package by using B3LYP/6-31G (d, p) basis set and the imperative results are summarized in Tables S3 and S4 (Supporting information). The molecular system has an intramolecular hyperconjugative interactions such as C1-O2 from N7 of n1(N7) $\rightarrow \pi^*$(C1-O2) where the electron density increases at 0.23363e weakening the related bonds C1-O2 which evidently exhibit strong delocalized designate with the stabilization of 54.47 kJ/mol; C5-O6 from N7 of n1(N7) $\rightarrow \pi^*$(C5-O6) and the electron

density increases in the range at 0.22975e weakening the related bonds C5-O6 amount to a stabilization of 53.57 kJ/mol; C5-N7 from n2(O6) → σ*(C5-N7) which increases the electron density 0.09310e and weakens the respective bonds C5-N7 leading to stabilization of 28.78 kJ/mol; C1-N7 from n2(O2) → σ*(C1-N7) increases the electron density 0.06774e and weakens the respected bonds C1-N7 which is related to stabilization energy of 28.48 KJ/mol; C4-C5 from n2(O6) → σ*(C4-C5) gives electron density at 0.0679e and the respective bonds weaken C4-C5, its lead to stabilization of 21.90 kJ/mol; C1-C3 from n2(O2) → σ*(C1-C3) shows the electron density as increasing at 0.06774e and weakens the particular bonds N7-C8 which have a stabilizing energy of 21.86 kJ/mol; N7-C8 from n1(N12) → σ*(N7-C8) which increases the electron density of 0.06540e and weakens the respective bonds C1-N7an account of stabilization of 10.79 kJ/mol. The natural hybrid orbital with higher energies, considerable p-characters are very close to almost (100%) and low occupation numbers such as n2 (O9), n1 (N7), π(C5-O6) and π(C1-O2). The energies, p-characters, occupation numbers of these orbitals are -0.27836, 0.26279,-0.37996 and -0.38072 a.u. and 99.88, 99.86, 99.83, 99.68, 99.82, 99.67 % and 1.86714, 1.58932, 1.98974 and 1.98968 a.u. The orbital with lower energies and high occupation numbers are n1 (O2), n1 (O9), (C5-O6) and (C5-N7). The energies, p-characters and occupation numbers of these orbital are -0.68199, -0.55564, -1.09022, -0.81121a.u. and 42.55, 55.14, 66.21, 57.02,69.71 and 66.70% and 1.97553, 1.96729, 1.99606 and 1.98581a.u. Thus, a very close to pure p-type lone pair orbital involve in the electron contribution to the σ*(C10-C11) orbital for n2(O9) → σ* (C10-C11) , π^*(C1-O2) orbital for n1(N7) → π^*(C1-O2), π^*(C5-O6) orbital for $n_1(N_7)$ → π^*(C5-O6), π^*(C5-O6) orbital for C5-O6→ π^*(C5-O6) and π^*(C1-O2) orbital for C1-O2→ π^* (C1-O2).

4.6. NMR Spectral analysis

The chemical shift analysis is the most significant technique adopted with design of molecular geometry dimension essential for consistent calculations of magnetic properties, after performing the full geometry of respected molecule. The ^{1}H and ^{13}C chemical shift values in GIAO, related to TMS (act as a reference for title compound) were predicted by using B3LYP/6-31G (d, p) level of theory; synchronize with the observed experimental values. The experimental ^{1}H and ^{13}C NMR spectra of the SMF molecule in DMSO solvent are presented in Fig.3 (a) and (b) respectively. The computed chemical shift values are in conformity with the corresponding experimental data. The results are summarized in Table 3.

4.6.1.^{1}H NMR spectrum of SMF

The hydrogen atoms of the N-CH_2-N group appear as singlet and the value was observed at higher chemical shift of 4.21 ppm (DMSO) due to influence of nitrogen atom with theoretical peaks at 4.68 ppm. The triplet at 3.52 ppm in the ^{1}H NMR spectrum of this compound shows the presence of methylene proton (N-(CH_2)2) having the coupling constant value of 4.75 Hz. The ^{1}H NMR spectrum of SMF reveals a doublet at 2.44 ppm for four protons attached to an oxygen group with the integral value corresponding to four protons having the coupling constant of 4.5Hz. A multiplet peak was observed at 2.51 - 2.50 ppm with four protons such as 15H, 16H, 17H and 18H (O=C-CH_2). A multiplet was appeared in the region of 2.51 - 2.50 ppm with four protons having the integral value which is always assigned to the succinimide ring protons. The DMSO (solvent) peak was observed at 3.3 ppm as shown in Fig.3 (a).

4.6.2.^{13}CNMR spectrum of SMF

In ^{13}C NMR spectrum, the progress of electrons from the oxygen atom having lone pair to non-bonding σ orbital due to the existence of carbon atom in the carbonyl group has low lying excited state, which produces a paramagnetic current [46]. This n- σ* produces a higher to a lower intensity, since the carbonyl carbon peaks occur due to the presence of higher wavenumber and it can appear in the range from 150-220 ppm [47, 48]. Thus, it has helped to identify the chemical shift value of a carbonyl group from the rest of the resonances, for the SMF molecule the carbonyl group has absorption at 179.13 ppm, which was compared with calculated value of 159.32 ppm in gas phase and 163.26 ppm in solvent (DMSO). In ^{13}C NMR spectrum of SMF, the absorption of seven aliphatic carbons give signals in the region 28.64 to 66.51 ppm, the peak at 28.64 ppm is due to the carbon(C4) attached to the carbonyl carbon which was compared with the computed value at 23.69 ppm in the gas phase and 20.55 ppm in DMSO solution. The electronegative atom of oxygen, attached to carbon C10 and C14 shows a higher wavenumber, thus the NMR signal was observed in the downfield at 66.51 and 59.69 ppm and the NMR signal was calculated at 59.80 and 58.84 ppm in gas phase and in solvent phase at 54.56 & 53.71ppm. The electron withdrawing atom present in the adjacent position, gives the chemical shifts in the de-shielded region. The signals at 40.48 and 40.31 ppm are related to the carbon C11 and C13 respectively show a deviation of theoretical value at 48.27 and 46.73 in gas phase and 43.32 and 41.91ppm in solvent (DMSO) phase. The highest electronegative property present in the nitrogen (N) atom gives the electron contribution around the bond to polarise through the neighbouring carbon atom; the electron density was found decreased at the association for the

SMF molecule. Therefore, the results seem to have slightly higher value for the SMF molecule under study at 50.90 ppm (C8) as predicted with the theoretical value at 52.81 in the gas phase and 48.99 in solvent (DMSO) phase. The DMSO (solvent) peak was observed at 40.24 - 39.48 ppm as shown in Fig.3 (b).

4.7. Mass spectrum of SMF

Mass Spectrum of SMF analysis was done with the HRMS method. In general, the calculated mass was appeared at m/z 198.22 (high predominant) and 199.1083(less predominant). Similarly, in the experiment interestingly matching with less predominant, the base peak, at *m/z* 199.11, it is related to the most stability of the Molecular ion peak [$C_9H_{14}N_2O_3^+$] of our compound. It shows a peak at m/z 200.11 corresponding to [M+H] $^+$peak and as represented by protonated of molecular ion, on account of the fragment of $C_9H_{15}N_2O_3^+$. The ^{13}C, ^{15}N, and ^{33}S mainly contribute to the M+1 peak, of which the ^{13}C is the most significant. If the M is range up to 100%, hence the M+1 intensity/1.1% which gives an approximation for the quantity of carbon atom present in the molecule. The peak observed at m/z 209.09, due to the fragment [$C_4H_6N_2O_2^+$], indicates an isotope peak of carbon atoms. The peak appears at m/z 221.08, is related to the molecular ion with sodium metal ion [$C_9H_{14}N_2NaO_3$]$^+$. The two peaks observed at m/z170.10 and 181.11 have values corresponding due to the fragment of $C_8H_{14}N_2O_2$ and $C_9H_{18}N_2O_2$.The disintegration pattern proposes as a molecular mass of SMF as 199.11 and nitrogen rule is also related by this corresponding value. The mass spectrum of SMF molecule is shown in Fig. 4(a).

4.8. TGA and DSC studies of SMF

The simultaneous TGA and DSC method was used to find the thermal stability and decomposition behaviour of the SMF molecule. The TGA and DSC study found the heating at the rate of 10 ºC/min from surrounding temperature to 600ºC/min in nitrogen atmosphere as shown in Fig.4 (b) [49]. From the TGA curve it is clear that until the melting point (102ºC) is reached, there is absence of weight loss, since the material is represented as the unreality of crystallization solvent or contamination and the most definite thermal stability of SMF up to beginning of melting point. The flat response of TGA plot after its melting point indicates the thermal decomposition of SMF with the formation of reaction products [50]. It takes place in two stages, the first mass loss occurs at 270.6 ºC - 300 ºC and suffers 88.41% mass fraction loss, due to the liberation of volatile substances like morpholine ring. The next mass loss takes place at 320 to 600.3 ºC on the description of the volatile product like N-Succinimide and residue left about 96.34% found towards the end. The final residual carbon mass at 600.3

ºC represents the end of the composition reaction is 3.40%. The second broad exothermic peak appears at 275 ºC and after this stage the mass loss in TGA occurs gradually. The gradual mass loss represents the liberation of succinimide fragments [51]. The decomposition temperature found as 270.6 ºC in TGA graph, above its melting point, represents the thermal stability of the SMF molecule. The significant weight loss below 270.6ºC indicates the title SMF molecule as devoid of physically adsorbed water and water of crystallisation. The final residual carbon mass at 600.3 ºC indicates the last part of the composition reaction is 3.40%. From the graph, it is obvious that the sharp exothermic peak with an onset, peak maximum with offset appear at 100, 114.0 and120ºC. The exothermic peak related to the activity of the sample melting point liberating the facilitating the process of melting. The second board exothermic peak was shown at 270.6 ºC. The maximum peak value and height of the peak will be indicated by sample weight and possibly by encapsulation procedure, hence the poor thermal conduct produces lower peak height with broader peak [52, 53]. It is determined by the purity of the sample and to analyze the curve obtained by a DSC plot with its shape. The higher concentration of an impurity in a given sample lower the melting point and broader the range. In SMF molecule, the highest melting point and the sharpness of the DSC melting peak reveal that SMF has higher crystallinity and purity.

4.9. UV-Visible spectral analysis

The recorded UV-Vis spectrum of SMF molecule is shown in Fig. S1 (Supplementary Information) and computed absorbance, oscillator strength and transition assignment are shown in Table 4. This spectrum shows that absorbance maxima for SMF molecule is at 287 nm due to possibility of n- π * transition which involve the transfer of electron from non-bonded atomic orbitals along with carbonyl O-atom to the first molecular excited state of SMF. The frontier molecular orbital analysis considers the HOMO as comparatively having large orbital co-efficient due to N-atom with one set of the lone pair of electrons residing on its sp^3 hybridized orbitals. Consequently, the non-bonded orbital of the O-atom having lone pairs are equally responsible for the assorted approaches of electronic excitation in the absorbance of SMF. Furthermore, the UV-Vis spectrum of SMF is shown in Fig.S5 (supplementary information) has been simulated by the TD-DFT model. The calculated observed spectrum gives a broader peak; which is slightly deviated from the observed experimental results λ_{max} value of SMF. The computed UV-Visible absorbance maximum appeared at 275 nm. The discrepancy with the experimental and computed values might be due to the short sightedness of the chosen DFT model and expected tolerance limit of 12 nm.

The experimental results mainly depend on factors such as solvent, concentration, solvation effect and molecular interactions.

4.10. Frontier molecular orbital analysis

The HOMO-LUMO energy gap plays an important role in determining the chemical reactivity, chemical reactions and strength of the molecule, UV-Vis spectra, electrical and optical properties. The HOMO-LUMO band gap was analysed through conjugated molecule, which provides an important role of specific movement of electron take place through the end capping nucleophilic groups like electron-donor atom to the effective electrophilic groups like electron-acceptor atoms with pi-conjugated bridge. The strong electronic interaction through pi-conjugated path results in considerable ground state donor-acceptor assimilation the appearance of an electron transfer band in the electronic spectrum. Therefore, electron transport properties localized over the morpholine group of the pi-conjugated molecule in the electron-donor (HOMO) side of its electron withdrawing part (LUMO). The electrical transport properties of molecules, for investigating the most reactive position that take place in pi-conjugated systems and also gives a numerous number of reactions in the conjugated system were explained by using an energy band gap between HOMO and LUMO has been done. In SMF molecule, there are 53 valence electrons presented in molecular orbitals, which is the highest occupied molecular orbital (HOMO) having unsymmetrical properties (A) among the energy of about -5.56 and also for lowest unoccupied molecular orbital (LUMO) having energy with -0.30 eV. It consists of 280 molecular orbitals and the atomic orbitals, mostly distributions towards the HOMO and LUMO, can be visualized from Fig. 6(a) and the obtained data are summarized in Table 5. Evidently, the HOMO and the LUMO of SMF molecule are primarily having a linear mixer of atomic orbitals of nitrogen on morpholine ring and the two adjacent carbonyl atoms at positions 2 and 5 of succinimide ring. The band gap or excitation energy between the frontier molecular orbitals is determined as ΔE (LUMO-HOMO) and found to be -5.26 eV. The electronic transition of the λ_{max} computed wavelength by B3LYP/6-31G (d, p) method has been contributed of H→L (99%) followed by H-1→L (95%) and H→L+1 (98%) for the solvent (DMSO) phase. The Gauss Sum 3.0 software [32] is used to predict the group contribution of the molecular orbit (DOS) for the SMF molecule in the gas and solvent phase as shown in Fig.6 (a). The PDOS spectrum represents bonding and anti-bonding interaction, due to positive overlap population and negative overlap population analysis [54] are shown in Fig.6 (b). The HOMO orbital is found on the morpholine ring, methylene group of succinimide ring, CH_2 and C=O bond are represented as

(84%+9%+25%+3%+1%) and the LUMO corresponds to the succinimide ring, C=O and methylene group of succinimide ring with the contribution of (60%+30%+6%).

4.11 Reduced Density Gradient (RDG) analysis

The real space weak interaction, based on electron density and derivatives is approached by RDG analysis and it is developed by Johnson et al. [55]. It is a dimensionless quantity and the first gradient found in the literature.

$$RDG = (r) = \frac{1}{2(3\pi r^2)^{\frac{1}{3}}} \frac{\left|\Delta^2 \rho(r)\right|}{\rho(r)^{\frac{4}{3}}} \quad \text{----------} \quad (3)$$

The weak interaction is identified by analyzing by low electron density values. The plot of RDG vs ρ provides the presence of interaction strength. The λ_2 sign is used to differentiate the bond ($\lambda_2<0$) interactions from non-bonding ($\lambda_2 > 0$) interaction. The Multiwfn and VMD software [56, 57] are used to plot the RDG surface for the SMF molecule. The RDG = 0.1 in the molecular denote the molecule having repulsive shown in the Fig.7 and attractive interaction. The value near to zero on both sides denote the equal possibility of attraction and repulsion in the molecular system. The gradient isosurface are mention in colour by the values of (λ_2) ρ, which represent the interaction strength in the molecular system seen from colour ranging from blue to red (stronger attraction to repulsion). As we look refer Fig.7, the red colour represents the ring system which is responsible for steric effect, the green colour represents the van der Walls (VDW) interaction which denote that the electron in the region are low.

4.12. Thermodynamic simulation properties of SMF

According to the principles of statistical thermodynamics and the standard thermodynamic function such as heat capacities at constant volume (C_V), entropies (S), and enthalpy changes (E) for the SMF molecule were computed from the theoretical harmonic frequencies predicted from B3LYP/6-31G (d, p) basic set in the temperature range of 100 - 1000 K are given in the Table S5 (Supplementary Information). It can be evaluated that the all values in thermodynamic functions are found increasing with the temperature which varies from 100 to 1000 K due to the increase in molecular vibrations intensities with increase in temperature. From the computed data, the quadratic fitting equations have been derived along with their factors (R^2). By using these equations (4, 5, 6), we can predict the attributes at any point of temperature without further computational procedures. It is inferred from the results

that the thermodynamic parameters linearly depend on the temperature value. The correlations between the thermodynamic properties and temperatures T values are shown in Fig.S6 (Supplementary Information). The correlation equations are as follows:

$E = -0.025+0.187T-7x10^{-5}T^2$ ($R^2=0.998$) ---------- (4)

$C_V = 146.8+0.016T+6x10^{-5}T^2$ ($R^2=0.999$) ---------- (5)

$S = 61.41+0.193-4x10^{-5}T^2$ ($R^2=1$) ---------- (6)

They can be used to predict the thermodynamic energy function based on the theory of relationship with thermodynamic variables and used to evaluate the directions of chemical behaviour following the thermodynamics second law in the thermochemical field [58].

4.13. Molecular Electrostatic Potential (MEP)

Molecular electrostatic potential (MEP) designed with the space about the molecule due to species distribution, is very useful in interpreting and predicting reactive charges of electrophilic and nucleophilic reaction for the investigation of biological identification and intermolecular hydrogen bonding interaction. The electrostatic potential provides information to analyze the processes according to the identification in the region of the molecule, as in drug-receptor and enzyme-substrate interactions, since this is through possibilities that the both species primary distinguish from each other. The MEP plot display the most probable reactive path of the respected molecule for an interaction with electrophilic and nucleophilic charges, MEP of SMF molecule at the DFT/B3LYP method with 6-31G (d, p) basic set optimized geometry was calculated. Negative region generally represented as red colour which is due to the presence of electrophilic reactivity of the represented molecule, whereas the blue colour indicates nucleophilic reactivities which are related to the presence of positive electrostatic potential of respected molecules as shown in Fig.S7 (supplementary information). The electronegative atoms having lone pair are usually associated with the negative electrostatic potential region. From the MEP plot of the SMF molecule, the negative region of the electrostatic potential is in C=O groups of succinimide ring and the oxygen atom of morpholine ring which are electrophilic. The maximum electrostatic potential arises due to the positive region as well in the region due to the presence of the nitrogen atom and hydrogen atoms which are nucleophlic. The result of MEP provides that clear evidence for the biological activity of the SMF molecule.

4.14. Molecular docking studies

Molecular docking study is one of the recent virtual simulation techniques used to find the binding site of protein-ligand site. The PASS (Prediction of Activity Spectra) [59] online tool is used for prediction of protein for ligand interaction. In our study, the PASS online result is shown in Table S6 (Supplementary Information). For molecular docking, the high resolution fine crystal structure of tumour suppressor in lung cancer 1 (PDB ID: 2HE7) [60] is used. We utilized Auto Dock 4 software package. Initially the protein was kept ready with the help of Auto Dock tools graphical [61] user interface. The polar hydrogen atoms were added to the protein, atomic charges were calculated by kollman method and lamarckian genetic algorithm (LGA) was utilized for molecular docking calculation implemented in Auto dock 4.0 software package [62]. The ligand PDB molecule was created by using the optimized molecular geometry. The active site to the energies was defined to add the residues of active site with the use of grid size 80Å×80Å×80Å using Autogrid [63, 64]. With the help of Auto Dock software [62] the binding energy (Kcal/mol), inhibition constants (µM), intermolecular energy (Kcal/mol) were computed in Table S7 (Supplementary Information), The best result i.e lowest binding result is shown in 2HE7 protein exhibit the lowest binding energy (-4.14 Kcal/mol) with inhibition constant value of 927.56 (µM) as shown in Table S8 (Supplementary Information). In Fig.8, the yellow dotted line implies the formation of hydrogen bonds of ligand with target proteins, hydrogen bond involved in the protein - ligand is illustrated using pymol software [65]. The analysis shows the point that lung cancer amino acid of LYS187, ASP149, LYS148, LEU153 form H-bond with C=O and O of title ligand with hydrogen bond length of 2.0, 2.9, 3.4 and 2.4 Å shows the existence of the ligand-protein interaction as shown in Table S8(Supplementary Information). The obtained finding from the PASS online and our computed result molecule might have potential inhibitor against the lung cancer protein.

5. Conclusion

The derivative of novel mannich base SMF molecule was synthesized and it has been characterized using vibrational, NMR, UV- Vis, mass and TG/DSc techniques. The DFT computations were used to predict the structural geometry and vibrational frequencies. The FT-IR recorded spectrum was investigated with the aid of Density Functional obtained from both experimental and theoretical studies confirming the presence of CO, C-O-C, and N-CH_2-N functional group. In the UV, the λ_{max} values of the SMF molecule were nearly similar in the liquid and gas phases, indicating the implications of optical activity of the molecule in the solvent as negligible. The DFT calculation with higher basis set predicted the Raman shifts as

especially a good deal compared to the experimental data. The HOMO was restricted over the morpholine ring except the succiniminide ring, whereas the LUMO was presented over the succinimide ring which resulted in the electron transfer process in molecular orbital. The MEP plot of the SMF molecule and negative region was mainly around over the C=O groups of succinimide ring and the oxygen atom of morpholine ring which were represented as electrophilic. The highest positive region was presented on the Nitrogen atom and hydrogen atoms which indicated as nucleophlic. The molecular docking study concludes with the fact that the SMF molecular has might inhibitor activity against protein, which indicates against the lung cancer as evident from the binding energy of-4.14 Kcal/mol. This result identifies the inhibitory activity against lung cancer disease.

Reference

[1] R.Wijtmans, M.K.S. Vink, H.E. Schoemaker, F.L. van Delft, R.H. Blaauw,F.P.J.T. Rutjes, Synthesis 5 (2004) 641- 662.

[2] T.X. Meitro, A. Cochi, D.G. Pardo, J. Cossy, J. Org. Chem. 76 (2011) 2594- 2602.

[3] R.J. Lukas, A.Z. Muresan, M.I. Damaj, B.E. Blough, X. Huang, H.A. Navarro,S.W. Mascarella, J.B. Eaton, S.K. Marxer-Miller, F.I. Carroll, J. Med. Chem. 53 (2010) 4731-4748.

[4] X. Sun, L. Niu, X. Li, X. Lu, F. Li, J. Pharm. Biomed. Anal.50 (2009) 27- 34.

[5] F. Micheli, S. Cremonesi, T. Semeraro, L. Tarsi, S. Tomelleri, P. Cavanni, B. Oliosi,E. Perdona, A. Sava, L. Zonzini, A. Feriani, S. Braggio, C. Heidbreder, Bioorg. Med. Chem. Lett. 26 (2016) 1329- 1332.

[6] P. Ghosh, M.J. Deka, A.K. Saikia, Tetrahedron 72 (2016)690-698.

[7] H. Takahata, S. Takahashi, S.I. Kouno, T. Momose, J. Org. Chem. 63 (1998) 2224 - 2231.

[8] J.M. Betancort, C.F. Barbas,Org. Lett. 3 (2001) 3737-3740.

[9] R. Dave, N.A. Sasaki, Org. Lett. 6 (2003) 15-18.

[10] S. Mayer, B. List, Angew. Chem.Int. Ed. 45 (2006) 4193-4195.

[11] Y.C. Quin, L. Pu,Angew. Chem. Int. Ed. 45 (2006) 273-277.

[12] S.G. Nelson, K. Wang, J. Am. Chem. Soc. 128 (2006) 4232-4233.

[13] S. Moss_e, M. Laars, K. Kriis, T. Kanger, A. Alexakis, Org. Lett. 8 (2006) 2559-2562.

[14]V.A.Sedavkina, I.V.Lizak, L.K .Kulikova et al ZhKhimfarm 1 (1984) 54–56.

[15] G.Y. Argay, J. SeresActaCrystallogr B 29 (1973) 1146-1149.

[16] W. Kwiatkowski, J. Karolak-Wojciehowska, J. Obniska, A. Zejc,ActaCrystallogr C 46 (1990)108- 112.

[17] W.Kwiatkowski, J. Karolak-Wojciehowska, ActaCrystallogrC 48 (1992) 206 -208.

[18]J.Karolak-Wojciehowska, W. Kwiatkowski, J. Obniska, A. ZejcActaCrystallogr C 52 (1996) 1808 -1810.

[19] W. Kwiatkowski, J.Karolak-Wojciehowska, ActaCrystallogrC 46 (1990) 913 -915.

[20] T.H. Koch, B.L. Barthel, B.T. Kalet, D.L. Rudnicki, G.C. Post, D.J. Burkhart, Anthracycline formaldehyde conjugates and their targeted prodrugs, Topics in current chemistry, 283 (2008) 141-170

[21]P. Sakthivel, P. S. Joseph, A. Sebastiyan, M. Y. Suvaikin,M. Ramesh ActaCryst. E63 (2007)o4143

[22]M. Ramesh Ijppr.Human, 6 (2016)230-240

[23]S. Rajeswari,G. VenkatesaPrabhu, D. Tamilvendan, V. Ramkumar, J Chem. Crystallogr. 40 (2010) 437–442

[24] M.J. Frisch, G.W. Trucks, H.B. Schlegel, G.E. Scuseria, M.A. Robb, J.R. Cheeseman, G. Scalmani, V. Barone, B. Mennucci, G.A. Petersson,H. Nakatsuji, M. Caricato, X. Li, H.P. Hratchian, A.F. Izmaylov, J. Bloino, G. Zheng, J.L. Sonnenberg, M. Hada, M. Ehara, K.

Toyota, R. Fukuda, J. Hasegawa, M. Ishida, T. Nakajima, Y. Honda, O. Kitao, H. Nakai, T. Vreven,J.A. Montgomery Jr., J.E. Peralta, F. Ogliaro, M. Bearpark, J.J. Heyd, E. Brothers,K.N. Kudin, V.N. Staroverov, R. Kobayashi, J. Normand, K. Raghavachari,A. Rendell, J.C. Burant, S.S. Iyengar, J. Tomasi, M. Cossi, N. Rega, J.M. Millam,M. Klene, J.E. Knox, J.B. Cross, V. Bakken, C. Adamo, J. Jaramillo, R. Gomperts,R.E. Stratmann, O. Yazyev, A.J. Austin, R. Cammi, C. Pomelli, J.W. Ochterski,R.L. Martin, K. Morokuma, V.G. Zakrzewski, G.A. Voth, P. Salvador,J.J. Dannenberg, S. Dapprich, A.D. Daniels, €O. Farkas, J.B. Foresman, J.V. Ortiz,J. Cioslowski, D.J. Fox, Gaussian-09, Revision A.02, Gaussian, Inc., WallingfordCT, 2009.

[25] A.D. Becke, J. Chem. Phys. 98 (1993) 5648–5652.

[26] C. Lee, W. Yang, R.G. Parr, Phys. Rev. B 37 (1988) 785–789.

[27] M.H. Jamroz, Vibrational Energy Distribution Analysis VEDA 4, 2004. Warsaw.

[28] R. Dennington, T. Keith, J. Millam, GaussView, Version 5, SemichemInc.,Shawnee Mission, KS, 2009.

[29] E.D. Glendening, A.E. Reed, J.E. Carpenter, F. Weinhold, NBO Version 3.1 Program Manual, TCI, University of Wisconsin, Madison, 1998.

[30] S.N. Azizi, A.A. Rostami, A. Godarzian, 29Si NMR chemical shift calculation forsilicate species by Gaussian software, J. Phys. Soc. Jpn. 74 (5) (2005)1609-1620.

[31] C.M. Rohlfing, L.C. Allen, R. Ditchfield, Proton and carbon-13 chemical shifts:comparison between theory and experiment, Chem. Phys. 87 (1) (1984) 9-15.

[32] N.M. O'boyle, A.L. Tenderholt, K.M. Langner, Cclib: a library for packageindependent Computational chemistry algorithms, J. Comput. Chem. 29 (5)(2008) 839 - 845.

[33] S. Shen, G.A. Guirgis, J.R. Durig, Struct. Chem. 12 (2001) 33-43.

[34] D. Michalska, R. Wysokinski, Chem. Phys. Lett. 403 (2005) 211-217.

[35] V. Arjunan, T. Rani, K. Santhanalakshmi, S. Mohan., Spectrochim.Acta A79 (2011) 1386 - 1394.

[36] A. K. Sachan, S. Chand, R. Srivastava, V. K. Shukla, S. K. Pathak, A. Kumar, O. Prasad , L. Sinha., J. Chem. Pharm. Res., 2014, 6(11):211-227.

[37] A.P.Scott, L.Radom, J.phys.chem 100 (1996) 16502 – 16513.

[38] L. Pauling ,CornellUniv.Press, New York (1948) 175.

[39]W.W.Coblent, Phys Rev Series-I 20 (1905) 273-291.

[40] M. Silverstein, G. Clayton Basseler, C.Morill, Wiley, New York, 1981

[41]N.Sundaraganesan, H. Saleem, S. Mohan, M. Ramalingam, V. Sethuraman, Spectrochim.Acta A 62 (2005) 740.

[42] L.J. Bellamy, The Infrared Spectra of ComplexMolecules, John Wiley, New York,1959.

[43] P.J. Kruegar, J. Jan, H. Wieser, J. Mol. Struct. 5 (1970) 375–387.

[44] N. Herlin, J. Bohn, C. Reynand, M. Cauchetier, A. Galvez, J.N. Rouzaud, Astron. Astrophys. 336 (1998) 1127–1131.

[45] D. Sajan, J. Binoy, B. Pradeep, K.V. Krishnan, V.B. Kartha, I.H. Joe, V.S. Jeyakumar, Spectrochim. Acta 60A (2004) 173–180.

[46] G.A. Jeffrey, J.R. Ruble, J.H. Yates, ActaCrystallogr. 39B (1983) 388–394.

[47] A.G. Al-Sehemi, A. Irfan, Arab. J. Chem.Doi:10.1016/j.arabjc.2013.06.019.

[48] R.G. Parr, R.G. Pearson, J. Am. Chem. Soc. 105 (1983) 7512.

[49] R.G. Parr, L.V. Szentpaly, S.J. Liu, J. Am. Chem. Soc. 121(1999) 1922-1924.

[50] T. J.Beaulaa, I. H. Joeb, V.K. Rastogic, V. B. Jothya, Chem. Phys. Lett. 624 (2015) 93-101.

[51] R. Bottom, Oxford: Blackwell (2008)88–118.

[52]V.Logvinenko, L.Yudanova, N .Yudanov, G.Chekhova, J Therm Anal Calorim. 74(2003) 395–399.

[53]T.Hatakeyama, Z.Liu. Chichester:Wiley; 1998.

[54] P.Gabbot,Oxford: Blackwell; (2008) 1–50.

[55]M. Chen, U.V.Waghmare, C.M.Friend, E.Kaxiras, J.Chem.Phys. 109 (1998) 6854-6860.

[56]S .Johnson, P.M.Keinan, J.C. Sanchez, A.J. Garcia, W. Cohen, J. Yang, Anu Chem. Soc.132 (2010) 6498-6506

[57] T.Lu, F.Chem, J.Comput. Chem. 33(2012) 580-592.

[58] W.Humphrey, A. Dalke, K.Schulten, J.Mol.Graph. 14 (1996) 33-38.

[59] LeenaSinha, Mehmet Karabacak, V. Narayan, Mehmet Cinar, Onkar Prasad,109 (2013)298-307

[60] A. Lagunin, A.Stepanchikova, D.Filimonov, V.Poroikov, PASS: Prediction of activity Spectra for Biologically Active Substances, Bioinformatics, 16 (2000) 747-748.

[61] R.D.Busam, A.G.Thorsell, A. Flores,M.Hammarstrom, C. Persson, B. Obrink, B.M. Hallberg, J.Biol.Chem. 286 (2011) 4511-4516.

[62] Tonthat, N.K., Juvvadi, P.R., Zhang, H., Lee, S.C., Venters, R., Spicer, L., Steinbach, W.J., Heitman, J., Schumacher, M.A. 7 (2016) 492-516.

[63] G.M. Morris, D.S.Goodsell, R.S.Halliday, R.Hurey, W.E.Hart, R.K.Belew, A.J.Olson, J.Comput.Chem. 19 (1998) 1639.

[64] M.M. Garrett, S.G. David, S. H. Robert, H. Ruth, E.H. William, K.B. Richard, J.O.Arthur, J. Comput. Chem. 19 (1998) 1639-1662., AcsChem.Biol., 11 (2016) 1710-1719.

[65] H. Ruth, M. M. Garrett, J.O. Arthur, S.G. David, J. Comput. Chem. 28 (2007) 1145-1152.

Table 1
Geometrical parameters [bond length (Å), bond angle (°) and dihedral angle (°)] of the SMF molecule.

Bond length	B3LYP/6131-G (d, p)	XRD[a]	Bond angle	B3LYP/6131-G (d, p)	XRD[a]	Dihedral angle	B3LYP/6131-G (d, p)	XRD[a]
			O2-C1-C3	127.4	127.3	O2-C1-C3-C4	-178.3	176.2
C1-O2	1.215	1.201	O2-C1-N7	124.7	124.3	C2-C1-C3-H15	59.8	
C1-C3	1.527	1.498	C3-C1-N7	107.8	108.4	C2-C1-C3-H16	-56.3	
C1-N7	1.392	1.387	C1-C3-C4	105.2	105.1	N7-C1-C3-C4	2	−4.5
C3-C4	1.537	1.510	C1-C3-H15	108.7	111.0	N7-C1-C3-H15	-119.9	
C3-H15	1.094	0.970	C1-C3-H16	108.7	111.0	N7-C1-C3-H16	124.0	
C3H-16	1.093	0.970	C4-C3-H15	113.5	111.0	O2-C1-C3-C5	178.0	−176.9
C4-C5	1.527	1.494	C4-C3-H16	113.7	111.0	O2-C1-N7-C8	2.4	−9.5
C4-H17	1.094	0.970	H15-C3-H16	107	109.0	C3-C1-N7-C5	-2.3	3.7
C4-H18	1.094	0.970	C3-C4-C5	105.1	105.2	C3-C1-N7-C8	-177.9	171.1
C5-O6	1.214	1.211	C3-C4-H17	113.7	111.0	C1-C3-C4-C5	-1.1	3.6
C5-N7	1.393	1.375	C3-C4-H18	113.4	111.0	C1-C3-C4-H17	-120.1	
N7-C8	1.473	1.482	C5-C4-H17	108.9	111.0	C1-C3-C4-H18	117.4	
C8-N12	1.444	1.430	C5-C4-H18	108.5	109.0	H15-C3-C4-C5	117.6	
C8-H19	1.094	0.970	H17-C4-H18	107	126.6	H15-C3-C4-H17	-1.4	
C8-H20	1.092	0.970	C4-C5-O6	127.6	109	H15-C3-C4-H18	-123.9	
O9-C10	1.425	1.423	C4-C5-N7	107.8	124.4	H16-C3-C4-C5	-119.8	
O9-C14	1.425	1.409	O6-C5-N7	124.6	112.2	H16-C3-C4-H17	121.2	
C10-C11	1.531	1.497	C1-N7-C5	114	122.9	H16-C3-C4-H18	-1.4	
C10- H21	1.095	0.970	C1-N7-C8	123.2	123.6	C3-C4-C5-O6	-179.8	178.6
C10-H22	1.105	0.970	C5-N7-C8	122.6	116.7	C3-C4-C5-N7	-0.2	−1.6
C11-N12	1.467	1.449	N7-C8-N12	112.3	108.0	H17-C4-C5-O6	-57.6	
C11-H23	1.098	0.970	N7-C8-H19	105.6	108.0	H17-C4-C5-N7	122.0	
C11-H24	1.094	0.970	N7- C8-H20	105.6	108.0	H18-C4-C5-O6	58.5	
N12-C13	1.468	1.454	N12-C8-H19	112.6	108.0	H18-C4-C5-N7	-121.9	
C13-C14	1.531	1.495	N12-C8-H20	111.3	107.0	C4-C5-N7-C1	1.5	−1.31
C13-H25	1.098	0.970	H19-C8-H20	109.1	110.21	C4-C5-N7-C8	177.2	−168.6
C13-H26	1.094	0.970	C10-O9-C14	111.7	111.5	O6-C5-N7-C1	-178.8	178.5
C14-H27	1.105	0.970	O9-C10-C11	110.8	111.2	O6-C5-N7-C8	-3.2	11.2
C14-H28	1.095	0.970	O9-C10-H21	106.4	109.0	C1-N7-C8-N12	88.5	101.5
			O9-C10-H22	110	109.0	C1-N7-C8-H19	-34.6	
			C11-C10-H21	111.3	110.0	C1-N7-C8-H20	-150.1	
			C11-C10-H22	110.1	110.0	C5-N7-C8-N12	-86.8	−92.6
			H21-C10-H22	108.1	108.0	C5-N7-C8-H19	150.2	
			C10-C11-N12	111.9	109.8	C5-N7-C8-H20	34.7	
			C10-C11-H23	108.5	109.0	N7-C8-N12-C11	118.7	−62.2
			C10-C11-H24	111.5	109.0	N7-C8-N12-C13	-106.9	68.0
			N12-C11-H23	108.0	110.0	H19-C8-N12-C11	-122.3	
			N12-C11-H24	109.2	110.0	H19-C8-N12-C13	12.1	
			H23-C11-H24	107.6	108.0	H20-C8-N12-C11	0.5	
			C8-N12-C11	116.6	114.7	H20-C8-N12-C13	135	
			C8-N12-C13	116.1	115.2	C14-O9-C10-C11	-58.5	58.5
			C11-N12-C13	111.4	110.7	C14-O9-C10-H21	-179.7	
			N12-C13-C14	111.7	109.5	C14-O9-C10-H22	63.5	
			N12-C13-H25	108.2	110.0	C10-O9-C14-C13	58.6	−58.9
			N12-C13-H26	109.1	110.0	C10-O9-C14-H27	-63.5	
			C14-C13-H25	108.6	110.0	C10-O9-C14-H28	179.8	
			C14-C13-H26	111.3	110.0	O9-C10-C11-N12	54.6	−57.2
			H25-C13-H26	107.8	108.0	O9-C10-C11-H23	-64.5	
			O9-C14-C13	110.9	111.5	O9-C10-C11-H24	177.2	
			O9-C14-H27	109.9	109.0	H21-C10-C11-N12	172.8	
			O9-C14-H28	106.4	109.0	H21-C10-C11-H23	53.7	
			C13-C14-H27	110.2	109.0	H21-C10-C11-H24	-64.6	
			C13-C14-H28	111.3	109.0	H22-C10-C11-12	-67.3	
			H27-C14-H28	108.0	108.0	H22-C10-C11-H23	173.6	
						H22-C10-C1H24	55.3	

C10-C11-N12-C8	85.3	−171.5
C10-C11-N12-C13	-51.2	56.2
H23-C11-N12-C8	-155.3	
H23-C11-N12-C13	68.3	
H24-C11-N12-C8	-38.6	
H24-C11-N12-C13	-175.1	
C8-N12-C13-C14	-85.6	171.7
C8-N12-C13-H25	154.9	
C8-N12-C13-H26	37.9	
C11-N12-C13-C14	51.1	
C11-N12-C13-H26	174.6	
N12-C13-C14-O9	-54.7	57.7
N12-C13-C14-H27	67.3	
N12-C13-C14-H28	-172.9	
H25-C13-C14-O9	64.5	
H25-C13-C14-H27	-173.5	
H25-C13-C14-H28	-53.7	
H26-C13-C14-O9	-176.9	
H26-C13-C14-H27	-54.9	
H26-C13-C14-H28	64.8	

[a]Table from Ref[21 -23]

Table 2. Vibrational wavenumbers obtained for SMF at B3LYP /6-31G(d, p) method [harmonic frequency (cm^{-1}), IR_{int}($Kmmol^{-1}$), Raman Intensity (Arb Units)].

Mode nos.	Experimental Wavenumber(cm^{-1})		Theoretical Wavenumber (cm^{-1})			TED (≥10%) Assignments
	FT-IR	FT-Raman	B3LYP scaled	IR_{int}	Ram_{Int}	
1	3452 br					νCH(99)
2			3031	6.06	49.86	νCH(98)
3			3030	4.29	13.13	νCH(99)
4			3018	0.04	26.4	νCH(97)
5		3014s	3011	11.1	26.22	νCH(96)
6			3004	13.88	22.2	νCH(95)
7			2992	45.47	99.71	νCH(95)
8			2990	55.1	68.95	νCH(99)
9	2986ms	2986ms	2988	2.71	110.46	νCH(99)
10			2982	12.9	25.08	νCH(98)
11	2961ms	2958vs	2970	11.5	29.03	νCH(93)
12	2938vw	2944vs	2940	62.89	60.66	νCH(84)
13	2939w		2935	13.4	10.15	νCH(96)
14	2880ms		2870	81.13	77.08	νCH(94)
15	2867s	2861s	2862	26.3	8.22	
16	2810ms	2833w				
17	2747vw	2763w				
18	2697vw	2706vw				
19		2651vw				
20						
21	2546vw					
22						
23	2269vw					
24	2168vw					
25	2080vw					
26	1966w					
27	1765s	1769vs	1800	30.51	34.32	νOC(86)
28	1737vs		1740	583.44	0.15	νOC(87)

29	1714vs					
30			1463	5.13	35.62	βHCH(62)
31			1458	3.81	10.32	βHCH(61)
32			1449	0.09	31.56	βHCH(89)
33			1443	5.07	44.55	βHCH(87)
34	1441vw		1442	5.9	49.28	βHCH(73)
35	1428vw	1434s	1424	30.72	20.3	βHCH(58)
36			1422	0.3	52.58	βHCH(90)
37	1393s	1391w	1396	55.92	7.22	τHCNC(49) + βCNC(10)
38	1387ms		1381	1.48	19.81	τHCOC(38) + γCHCH(28)
39	1362vw		1369	5.87	8.62	τHCNC(54)
40			1359	1.86	11.23	βHCN(34)+ τHCNC(13)
41	1349vs		1345	42.96	4.9	γHCCH(14) + βHCN(12)
42			1338	6.49	39.49	βHCN(56)
43	1324vs	1321ms	1320	34.67	13.11	τHCOC(17) + γCHCH(16) + τHCNC(13)
44		1308s	1319	306.42	9.32	τHCNC(26)+ βCNC(10)
45			1280	6.63	50.88	βHCO(71)
46			1274	28.31	0.58	βHCC(23)+ τHCCC(19)
47	1274vs		1271	89.56	7.16	τHCNC(15)
48	1245s		1235	33.64	11.97	βHCC(36)+ τHCCC(19)+τHCCN(16) + νCC(13)
49	1228w	1224vw	1228	1.33	4.65	βHCO(30)+ τHCOC(11)
50	1203s	1210vw	1205	0.43	31.07	βHCC(30)+ γCCCH(23)+τHCCC(11)
51		1196w	1194	37.68	28.25	βHCO(37)+βHCN(26)
52	1148vs	1140s	1139	61.66	20.94	νNC(14) + τHCNC(12) + γCCOH(10)
53	1133s		1133	48.58	8.53	νNC(32)
54	1121s		1124	1.91	9.58	βHCC(35)+τHCCC(19)+ τHCCN(12) + γCCCH(11)
55	1110vs		1103	66.76	3.07	νOC(75)
56	1072s	1070w	1066	72.85	15.54	νCN(22)+ γCCOH(10)
57	1059s		1061	31.26	1.69	γCCOH(21) + νNC(10)
58	1039s	1028s	1033	17.78	1.34	νCC(21)+ βHCN(13)
59			1013	2.08	7.24	νCC(36)+νCN(36)
60	1014vw	1014s	1011	37.32	4.16	βCCO(16) + νNC(11)+ βCCN(10)
61	1000w	999s	993	0.04	0.14	γCCCH(56)+ γOCNC(22)
62	985ms	984s	979	3.42	33.89	νCC(69)
63	934w		961	46.11	44.3	νOC(33)+νCC(37) + νNC(10)
64	883s	884s	893	7.58	10.58	τHCNC(11)
65	855vw	854s	853	20.15	1.09	νCC(46)
66			829	14.74	40.93	νOC(53)+ νCC(11)
67	821ms	826	824	0.19	11.54	νNC(21)+ γCCOH(16)
68			809	18.58	29.36	γCCCH(31)+ γOCNC(24)
69	781vw	783ms	780	6.88	72.22	νNC(58)+ βNCN(11)
70	732w	739vs	719	14.06	98.54	νCC(36) + βNCN(15) + νNC(13)
71	632vs	661vs	651	36.27	11.2	βCCC(74)

72	621w	608s	620	18.65	75.54	βCNC(27)+ νNC(23)+ βNCN(10)
73	585vw	589s	583	2.15	14.52	βCCO(18)+ βCNC(13)+γCCOH(12) + βCCN(10)
74	557w	561s	557	9.57	12.87	γOCNC(42)+ βCNC(10)+γCCCH(10)
75	547vw	546w	548	0.1	11.79	γOCNC(69) + γCCCH(11)
76	536vw	532w	540	0.19	28.98	βCCO(64) + νCC(27)
77	479w	474vw	470	0.07	25.99	βCCN(26) + βCNC(10)
78	467w		468	0.28	34.94	βCCN(31)
79			433	0.25	4.2	τNCCO(48) + βCCO(10)+ τHCNC(10)
80	428w	413w	430	0.77	11.59	τHCNC(49) + βCNC(10)
81			386	28.53	18.49	βCCO(47)
82	318vw	315w	312	14.83	3.89	τCOCC(31)
83	268vw	272w	271	3.51	6.93	τCOCC(26)
84	219vw	216vw	254	1.41	2.84	βCNC(34)+ τNCCO(20)
85	170vw	171vw	174	3.34	49.07	βCNC(40)+ τNCCO(27)
86	121vw	119vs	117	9.75	10.13	γNCCO(27)
87	96vw	99vw	100	4.09	56.91	τCCNC(43)+τCNCC(18) + βNCN(10)
88		76vs	84	0	6.48	τCCCC(86)
89		62vs	61	0.45	86.79	
90			34	0.02	147.04	τCNCN(83)
91			20	0.02	31.16	τCNCN(78)

IR_{int} - IR intensity; Ram_{Int} - Raman Intensity; $Kmmol^{-1}$ w-weak; vw- very weak; s-strong; vs-very strong; m-medium; br, sh- broad, shoulder, υ - stretching; υ_{sym} – symmetric stretching ; υ_{asy}- asymmetric stretching ; δ- in plane bending ; γ- out-of –plane bending ; τ- torsion.

Table 3.

The experimental and theoretical ^{13}C and ^{1}H NMR chemical shift values of the SMF molecule

	δcal		(δexp)		δcal		(δexp)
Atom	**Gas**	**DMSO**		**Atom**	**Gas**	**DMSO**	
C1	159.32	163.26	179.13	H15	2.37	2.60	2.51(m,4H)
C3	23.69	20.54	28.64	H16	2.43	2.62	2.51(m,4H)
C4	23.69	20.55	28.64	H17	2.38	2.59	2.51(m,4H)
C5	159.01	163.04	179.13	H18	2.45	2.63	2.51(m,4H)
C8	52.81	48.99	50.90	H19	4.75	4.68	4.21(s,2H)
C10	59.80	54.56	66.51	H20	4.53	4.50	4.21(s,2H)
C11	48.27	43.32	40.48	H21	3.60	3.56	3.52(t, J=4.75MHz,4H)
C13	46.73	41.91	40.31	H22	3.70	3.73	3.52(t, J=4.75MHz,4H)
C14	58.84	53.71	59.69	H23	3.25	3.19	2.44(t, J=4.5MHz,4H)
				H24	3.12	2.96	2.44(t, J=4.5MHz,4H)
				H25	3.14	3.10	3.52(t, J=4.75MHz,4H)
				H26	3.22	3.04	3.52(t, J=4.75MHz,4H)
				H27	3.82	3.84	2.44(t, J=4.5MHz,4H)
				H28	3.61	3.56	2.44(t, J=4.5MHz,4H)

Table. 4. Experimental and Calculated absorption wavelength, energies and oscillator strengths of SMF using the TD-DFT method at B3LYP/6-31G(d, p) method.

Excitation	CI expansion Coefficient	Wavelength λ (nm) Cal.Gas Phase	Oscillator Strength (f)	Excitation	CI expansion Coefficient	Wavelength λ (nm) Cal. DMSO	Oscillator Strength (f)	Expt.	Assignment	In Solvent [a]Major Contribution (≥ 10%)
Excited State 1				**Excited State 1**						
53→54	4.4933	276	0.0007	53→54	4.5068	275	0.0008	287	n→π*.	H→L (99%)
Excited State 2				**Excited State 2**						
49→55 52→54	5.1601	240	0.0011	52→54	5.2385	237	0.0013		π → π *.	H-1→L (95%)
Excited State 3				**Excited State 3**						
53→55	5.4958	226	0.0044	53→55	5.5993	221	0.0053		π → π *.	H→L+1 (98%)

[a]H-HOMO; L-LUMO

.

Table.5.
HOMO, LUMO, Kubo gap, global electronegativity, global hardness and softness, global electrophilicity index, and dipole moment of the SMF molecule

Parameters	Gas phase	Solvent phase (DMSO)
	B3LYP/6-31G (d,p)	**B3LYP/6-31G (d,p)**
HOMO	-5.56	-5.59
LOMO	-0.30	-0.31
ΔEHOMO - ELUMO gap	-5.26	-5.28
Ionization potential(I)	5.56	5.59
Electron affinity(A)	0.30	0.31
Chemical potential(μ)	-2.93	-2.95
Chemical hardness(η)	2.63	2.64
Electronegativity(χ)	2.93	2.95
Softness(σ)	281.47	280.44
Electrophilicity index(ω)	1.64	1.65
Dipole moment(Debye)	55.57	70.80
SCF Energy (Hartrees)	26131.62	26131.62

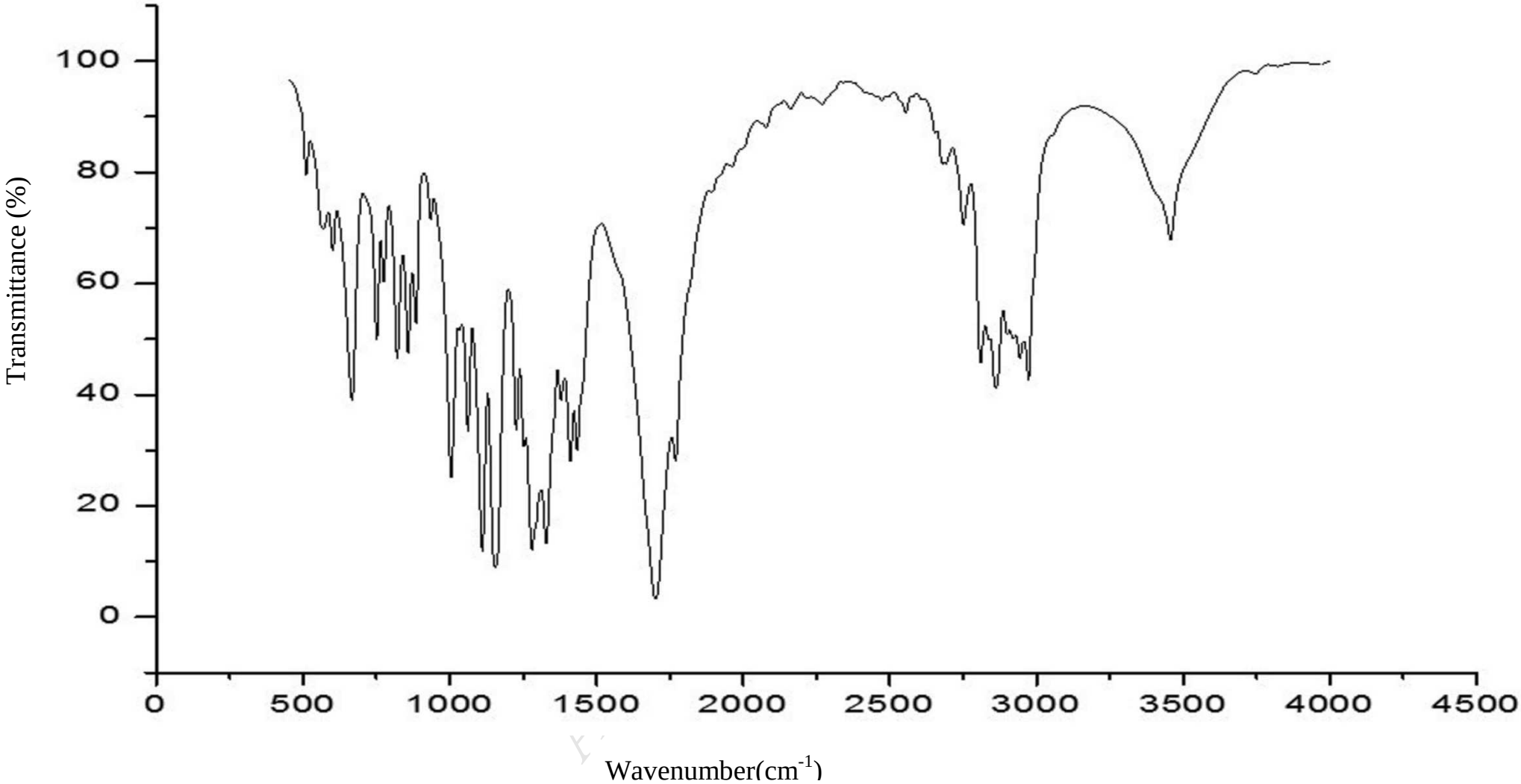

Fig.1. Experimental FT-IR spectrum of SMF molecule

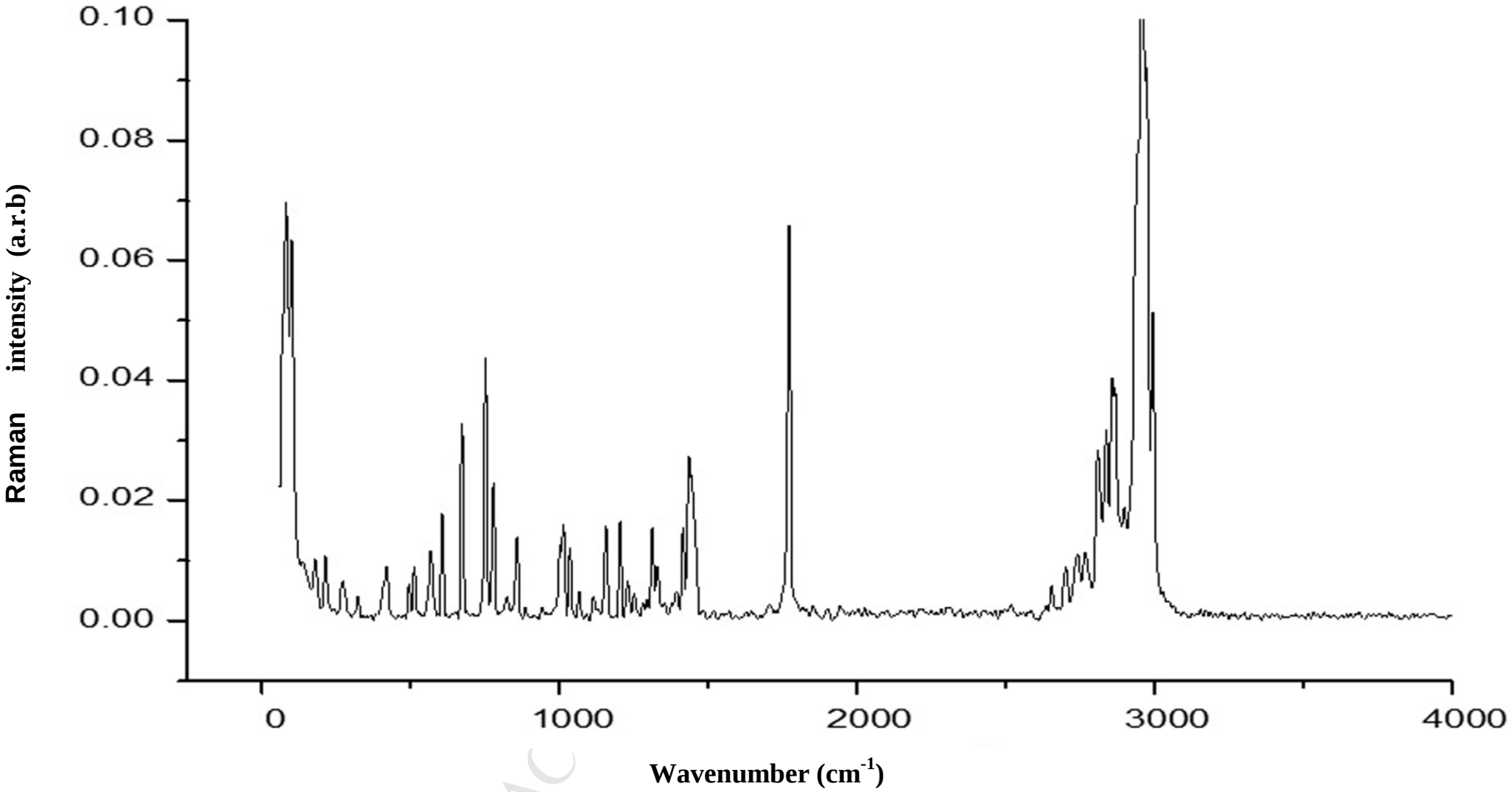

Fig. 2.Experimental FT-Raman spectrum of SMF molecule

(a)

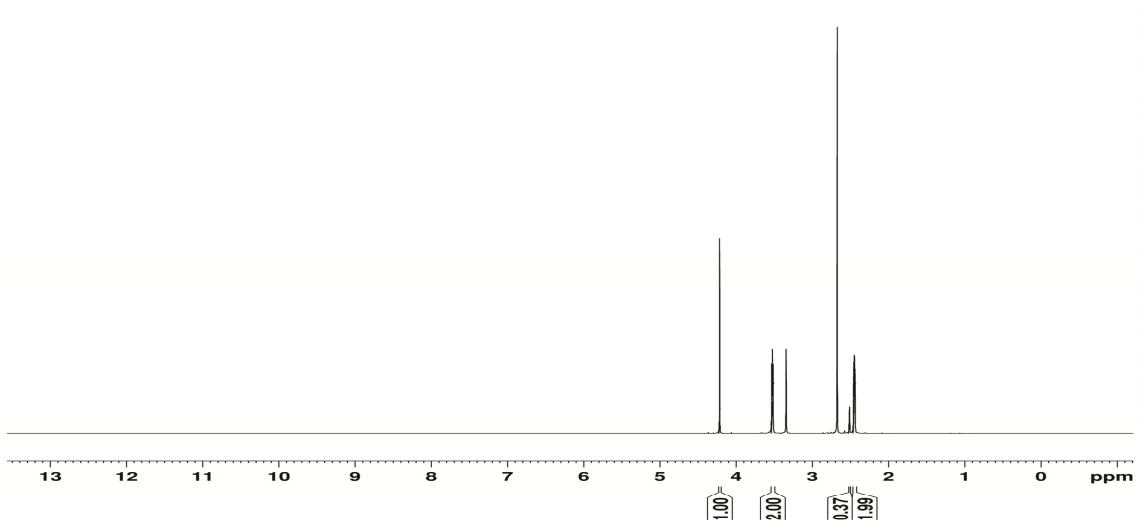

(b)

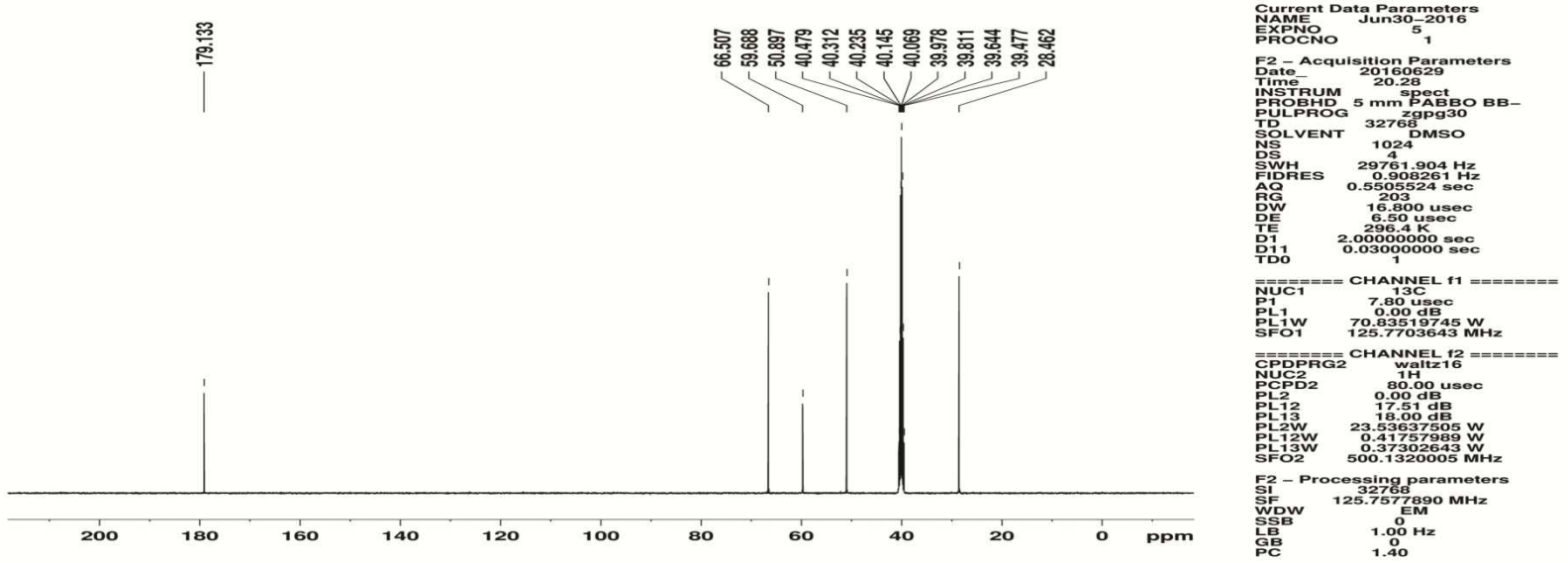

Fig.3. (a) ^{1}H NMR and (b) ^{13}C NMR spectrum of SMF molecule

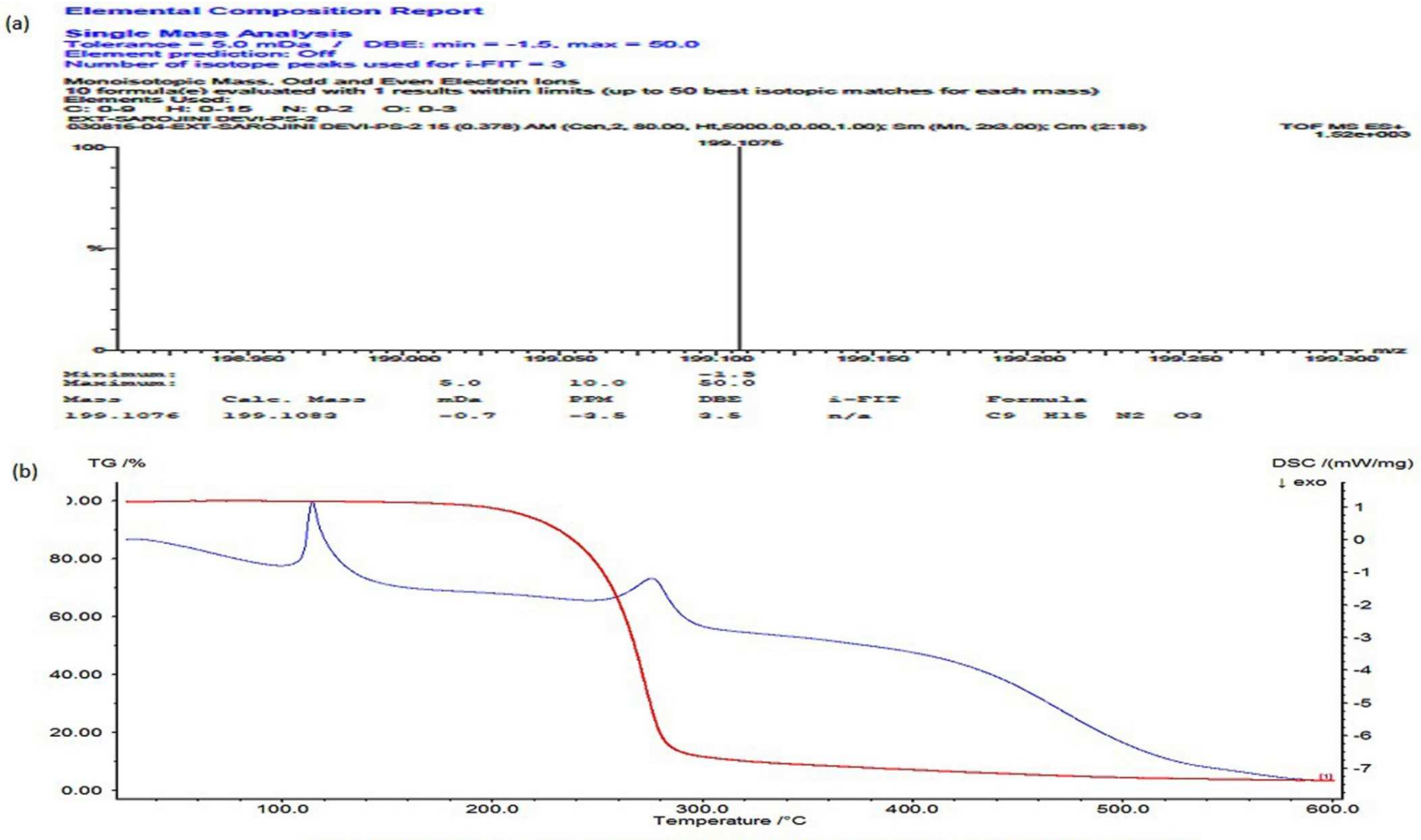

Fig.4. (a) Mass spectrum and (b) TG/DSC spectrum of SMF molecule

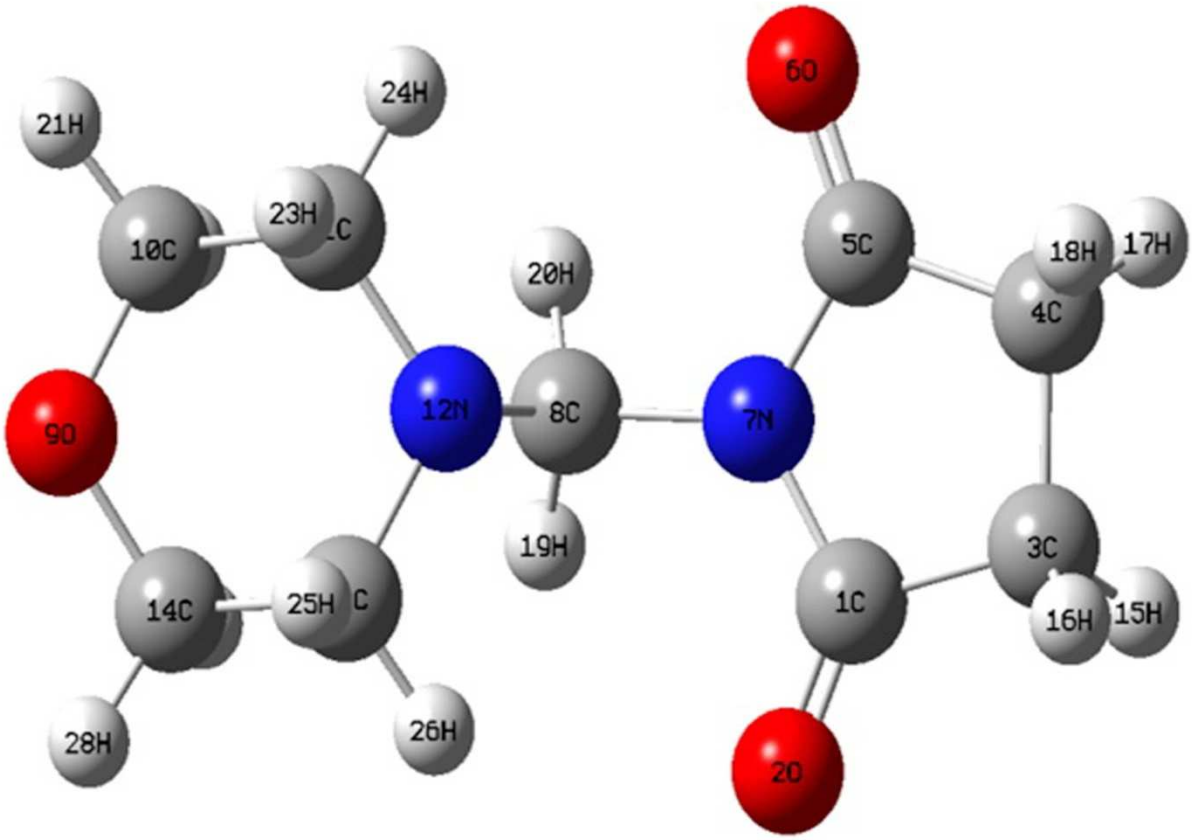

Fig. 5.Optimized geometry of SMF molecule

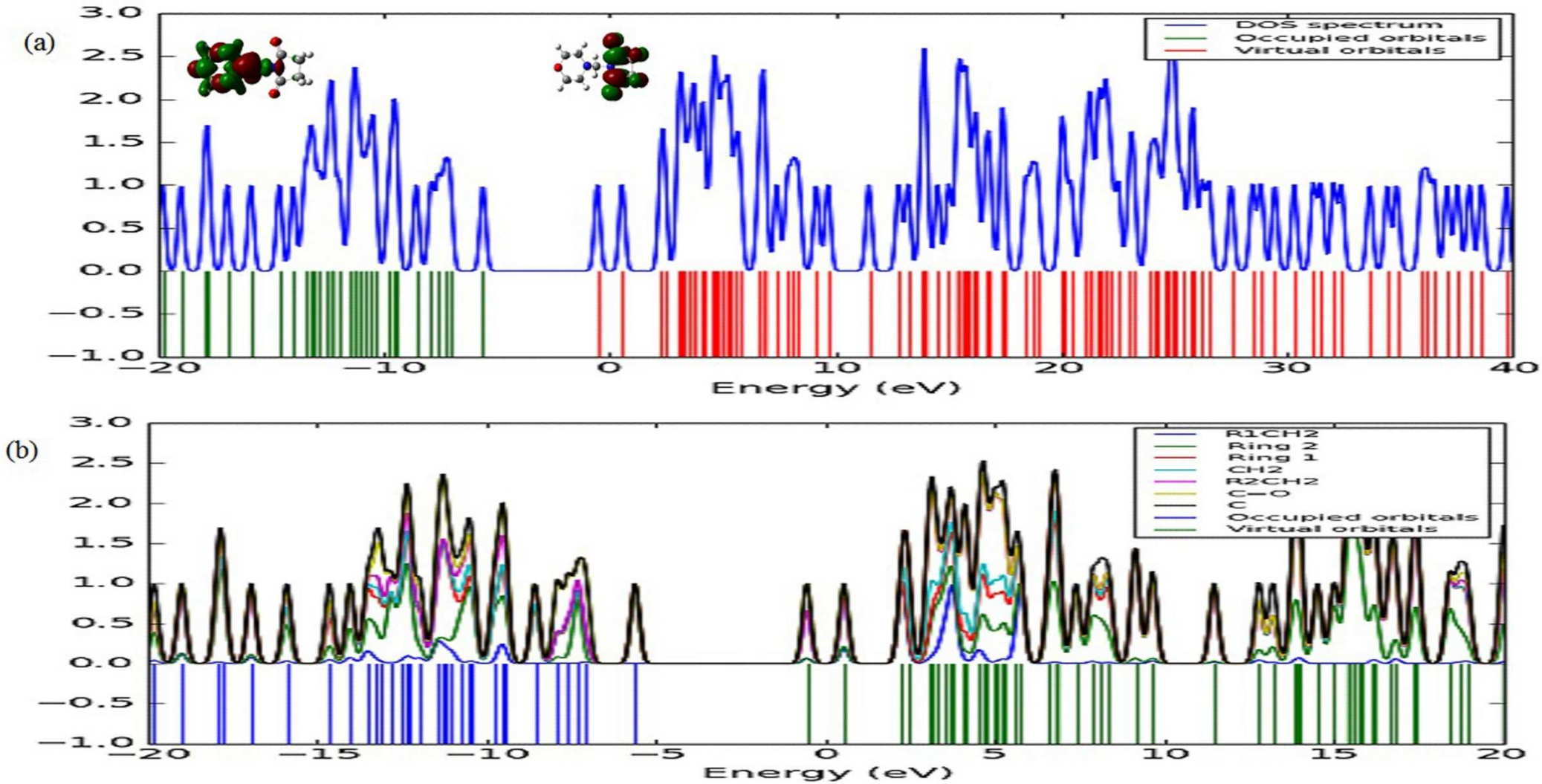

Fig.6. (a) HOMO-LUMO, DOS and (b) PDOS diagram of SMF molecule

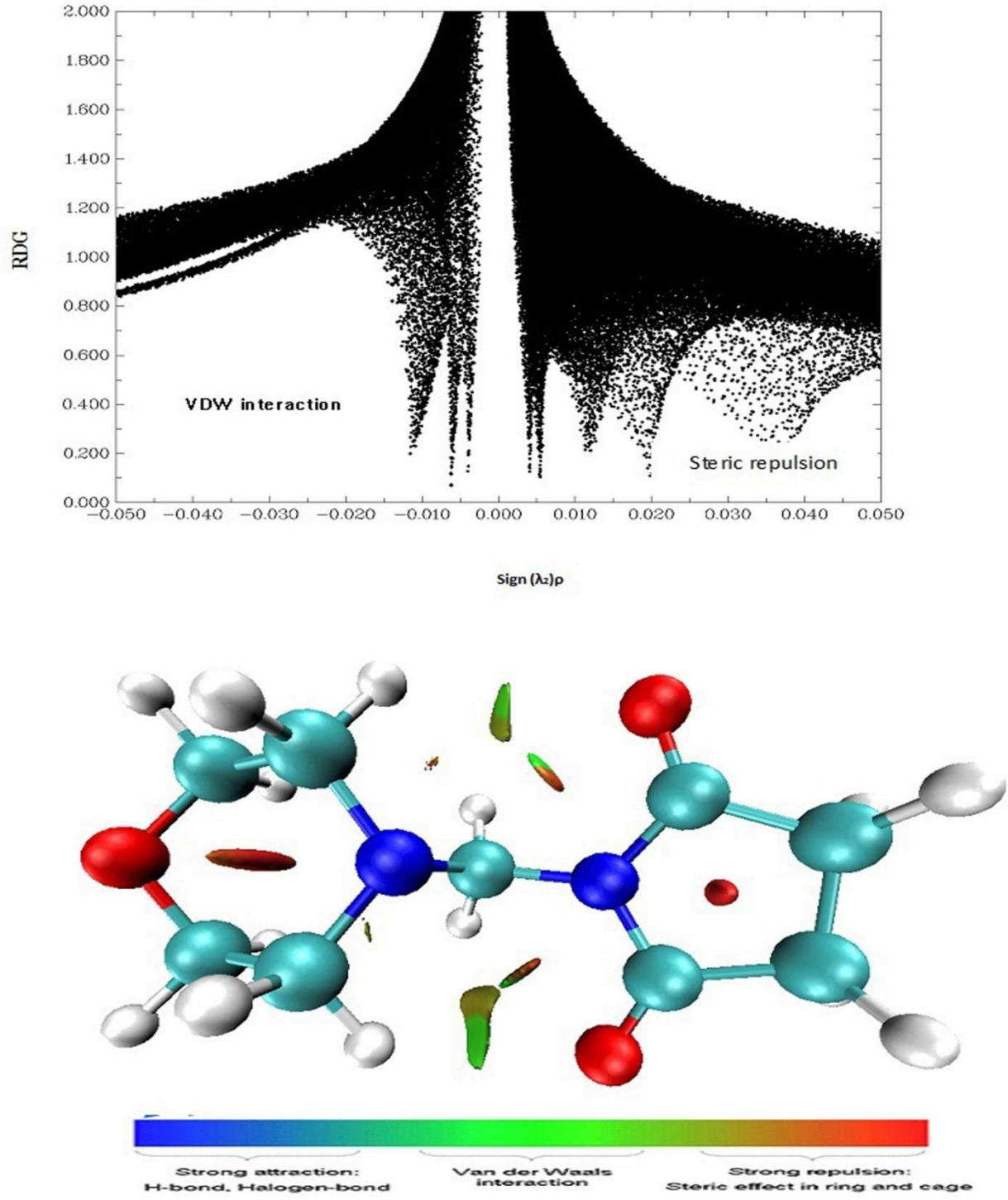

Fig.7. The Reduced Density Gradient of SMF molecule (Top) and Coloured surface of SMF molecule (Bottom)

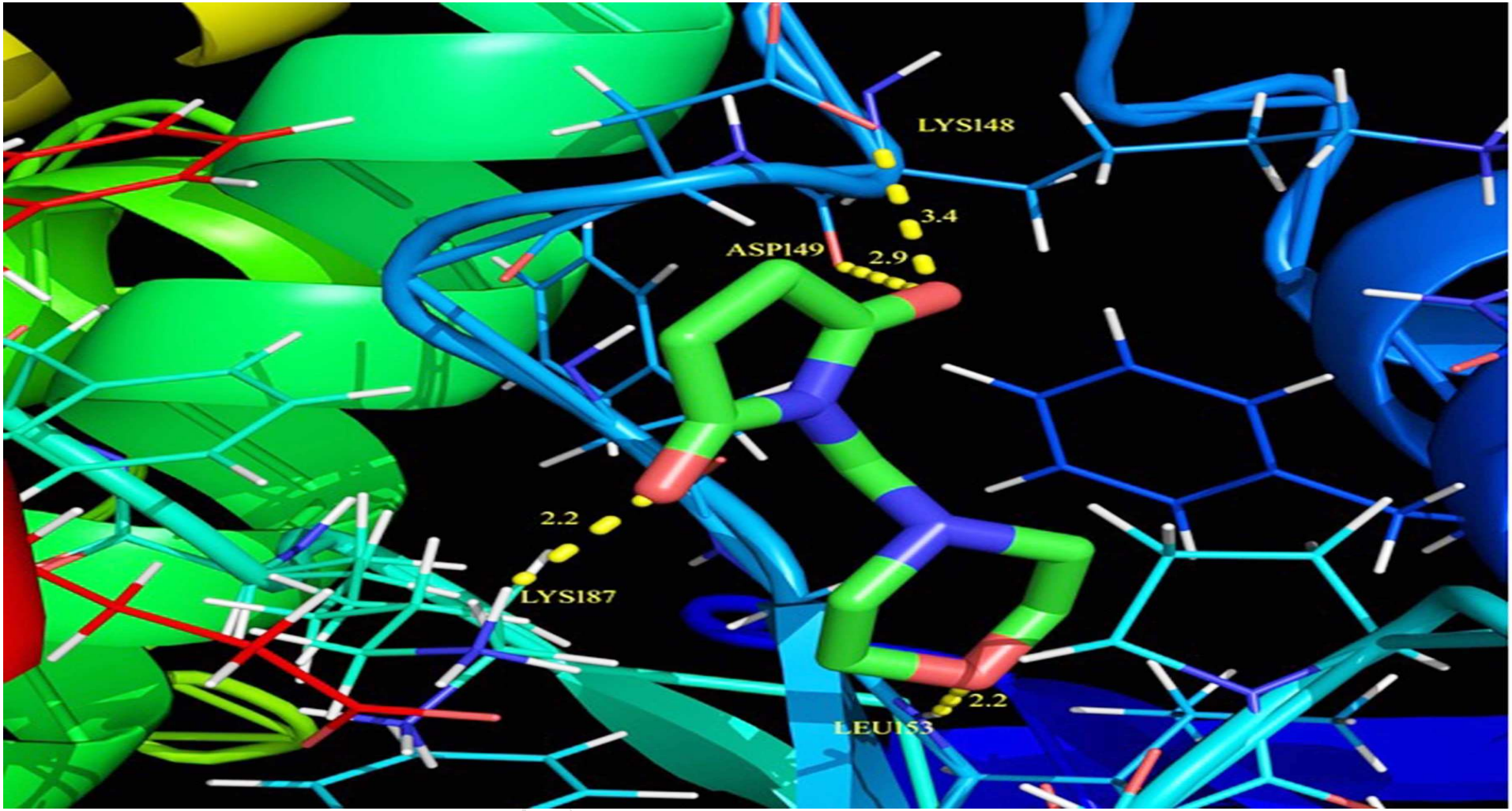

Fig.8. The binding site of SMF molecule with 2HE7 protein.

SMF was characterized by using spectroscopic techniques.

The H atoms and C atoms chemical shifts were analysed by NMR investigation.

PDOS and RDG spectrum have been performed.

Molecular docking studies suggest the SMF molecule might act as a lung cancer protein.